

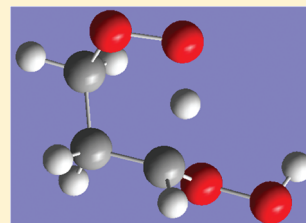
Role of $O_2 + QOOH$ in Low-Temperature Ignition of Propane.

1. Temperature and Pressure Dependent Rate Coefficients

C. Franklin Goldsmith,^{†,‡} William H. Green,[†] and Stephen J. Klippenstein^{*,§}[†]Department of Chemical Engineering, Massachusetts Institute of Technology, Cambridge, Massachusetts 02139, United States[‡]Department of Inorganic Chemistry, Fritz Haber Institute, Berlin 14195, Germany[§]Chemical Sciences and Engineering Division, Argonne National Laboratory, Argonne, Illinois 60439, United States

S Supporting Information

ABSTRACT: The kinetics of the reaction of molecular oxygen with hydroperoxyalkyl radicals have been studied theoretically. These reactions, often referred to as second O_2 addition, or $O_2 + QOOH$ reactions, are believed to be responsible for low-temperature chain branching in hydrocarbon oxidation. The $O_2 +$ propyl system was chosen as a model system. High-level ab initio calculations of the $C_3H_7O_2$ and $C_3H_7O_4$ potential energy surfaces are coupled with RRKM master equation methods to compute the temperature and pressure dependence of the rate coefficients. Variable reaction coordinate transition-state theory is used to characterize the barrierless transition states for the $O_2 + QOOH$ addition reactions as well as subsequent $C_3H_6O_3$ dissociation reactions. A simple kinetic mechanism is developed to illustrate the conditions under which the second O_2 addition increases the number of radicals. The sequential reactions $O_2 + QOOH \rightarrow OOQOOH \rightarrow OH + \text{keto-hydroperoxide} \rightarrow OH + OH + \text{oxy-radical}$ and the corresponding formally direct (or well skipping) reaction $O_2 + QOOH \rightarrow OH + OH + \text{oxy-radical}$ increase the total number of radicals. Chain branching through this reaction is maximized in the temperature range 600–900 K for pressures between 0.1 and 10 atm. The results confirm that *n*-propyl is the smallest alkyl radical to exhibit the low-temperature combustion properties of larger alkyl radicals, but *n*-butyl is perhaps a truer combustion archetype.



1. INTRODUCTION

Low-temperature autoignition of hydrocarbons is an essential component of advanced engine concepts that rely on compression ignition. As new or nontraditional fuels are developed, detailed chemical kinetic modeling is a useful tool for assessing combustion properties, such as pollutant formation and ignition properties. For these models to be practical, however, they must contain rate coefficients and branching fractions that are quantitatively accurate over a broad range of conditions and reactants. One of the most important classes of reaction in low-temperature ignition is the reaction of alkyl radicals with oxygen. A thorough review of experimental and theoretical work on this reaction can be found in Zádor et al.¹ Only an abbreviated summary is provided here.

The fundamentals of this complex reaction network are illustrated in Figure 1.

The alkyl radical, R , reacts with O_2 to form an energetically excited adduct, RO_2^\ddagger . This energetic adduct can stabilize, isomerize, or decompose to many channels, only four of which are generally relevant: alkylperoxy radical, RO_2 ; hydroperoxyalkyl radical, commonly called $QOOH$; cyclic ether + OH ; and alkene + HO_2 .

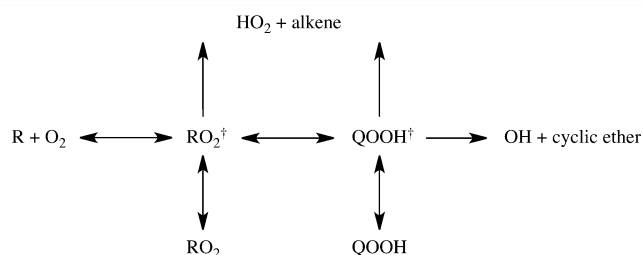
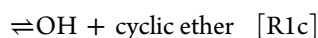


Figure 1. Reaction network for alkyl radical + O_2 . The superscript \ddagger denotes the vibrationally excited adduct.

At low temperatures, the $R + O_2$ reaction leads primarily to RO_2 . As the temperature increases, both chemically and thermally activated formation of alkene + HO_2 , $QOOH$, and cyclic ether + OH become competitive. At higher temperatures, alkene + HO_2 is the dominant product channel for the $R + O_2$ reaction, and the $R + O_2 = RO_2$ equilibrium shifts to favor $R + O_2$. These temperature variations in the $R + O_2$ reaction kinetics have a significant impact on the negative temperature coefficient region. Depending upon the temperature and pressure, the reactants can proceed directly to the various product channels on the same time scale as collisions without first being stabilized into the alkylperoxy radical. Similarly, the individual

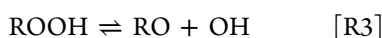
Received: November 8, 2011

Revised: January 16, 2012

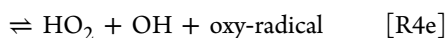
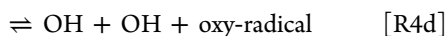
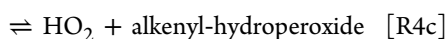
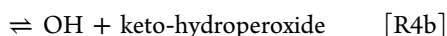
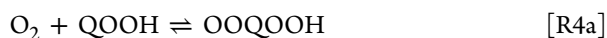
Published: January 17, 2012

RO₂ and QOOH isomers can decompose across multiple transition states directly to nonadjacent products. These formally direct (or well skipping) pathways are an essential component of the alkyl + O₂ reaction, and a rigorous, quantitative description of the temperature and pressure dependence of the rate coefficients can be obtained from the eigenvalue solution to the master equation.

Reactions R1a–R1d are chain propagating. As such, they are insufficient to explain the exponential growth in radical concentration during ignition. The conventional model for chain-branching in low-temperature, high-pressure oxidation involves RO₂ abstracting an H atom from a stable molecule (e.g., the parent hydrocarbon) to form an alkyl hydroperoxide, ROOH, which subsequently decomposes to an alkoxy radical, RO, and OH:



An alternative chain-branching sequence is the addition of oxygen to QOOH. Because the unpaired electron is located on a carbon atom, it can undergo a second O₂ addition to form a hydroperoxyalkylperoxy radical, OOQOOH. This species rapidly dissociates to form either OH + keto-hydroperoxide or HO₂ + alkenyl hydroperoxide. These bimolecular products also can be formed directly from the O₂ + QOOH reactants via chemical activation.



As with alkyl hydroperoxide decomposition, the O–OH bonds in the keto-hydroperoxides and alkenyl hydroperoxides are relatively weak, and these species can further decompose to OH + oxy-radicals at low temperatures. Consequently, the addition of a second O₂ to QOOH can be chain branching, because three radicals are produced for every radical consumed. Reaction R4d is of particular interest, because the two dissociation steps are below the reactants in energy; thus, it is conceivable that the O₂ + QOOH reactants can proceed directly to the OH + OH + oxy-radical products in a single step. The competing sequence, reaction R4e, is energetically less favorable and is unlikely to proceed as a single step.

For reactions R4a–R4e to be relevant, the QOOH precursor must first be present in sufficiently high concentrations. However, at low temperatures, equilibrium favors RO₂, and at high temperatures, equilibrium favors R + O₂. Because no QOOH has ever been observed experimentally, it is often debated whether or not QOOH concentrations are simply too low to matter. Nonetheless, various estimates of the O₂ + QOOH rate constants have been included in oxidation mechanisms for decades (see, for example, the mechanisms of Lawrence Livermore National Lab² and the National University of Ireland, Galway³).

The QOOH radical is formed by [R1b] and by isomerization of thermalized RO₂ [R5].



The most energetically favorable transition states for this isomerization reaction involve six- and seven-membered rings. Although three-, four-, and five-membered ring transition states exist, they are energetically unfavorable. For example, the barrier height for isomerization from ethylperoxy to hydroperoxyethyl in the O₂ + C₂H₅ reaction is above the reactants in energy; therefore, O₂ + QOOH reactions do not play a significant role in ethyl ignition.⁴ For the O₂ + *n*-propyl reaction, in contrast, the transition state for isomerization from *n*-propylperoxy to 3-hydroperoxypropyl proceeds via a six-member ring, with a barrier height that is nearly ten kcal/mol below the reactants in energy.⁵ Thus, *n*-propyl is the smallest alkyl radical that exhibits the key ignition properties of larger alkyl radicals, and as such is often described as the combustion archetype.⁶

One of the great challenges in oxidation chemistry is determining accurate rate coefficients for radical–radical reactions. For many radical–radical reactions, there is no saddle point on the dividing surface between products and reactants. As a consequence, the usual approach of computational kinetics, using a rigid-rotor harmonic-oscillator model to compute the transition-state properties at the saddlepoint, cannot be used. Instead, variational transition-state theory must be used to minimize the reactive flux. For a review of computational techniques for radical–radical reactions, the reader is directed to refs 7 and 8. Because molecular oxygen is a ground-state triplet, it behaves like a radical in R + O₂ reactions, and these reactions are barrierless. The intrinsic difficulties in computing suitably accurate rate coefficients for barrierless reactions have hindered the development of kinetic mechanisms for these important reaction systems. The difficulties in determining the rate coefficients for O₂ + QOOH, coupled with the uncertainty regarding QOOH concentrations, are the main reasons why these reactions have not been studied in detail in the literature.

The O₂ + *n*-propyl reaction has been studied extensively (see ref 1 and references therein). We limit our discussion to results obtained within the past ten years, with an emphasis on the time-resolved spectroscopic measurements of radical concentrations of Taatjes and co-workers at the Combustion Research Facility at Sandia National Laboratory. DeSain et al.^{4,5,9} measured HO₂ and OH profiles from the Cl-initiated oxidation of propane. The corresponding C₃H₇O₂ potential energy surface (PES) was computed using an MP2 basis set corrected QCISD(T)/6-311G(d,p)//B3LYP/6-31G(d) level of theory. The barrierless entrance channels were calculated using variational transition-state theory, based upon B3LYP/6-31G* reaction path energies. RRKM and Master Equation (ME) equation calculations were performed for both O₂ + *n*-propyl and O₂ + isopropyl.

The HO₂ concentration measured by DeSain et al. was characterized by a prompt yield and a slower growth, which is consistent with a combination of the (fast) formally direct O₂ + *n*-propyl → HO₂ + propene channel and the (slow) sequential O₂ + *n*-propyl → *n*-propylperoxy → HO₂ + propene channel, as well as the corresponding O₂ + isopropyl reactions. The potential energy surface was modified within the error bounds of the computational methods to improve the fit with the experimental data. The experimentally observed OH profiles could not be fit as accurately. The model underpredicted the OH yield at higher temperatures and overpredicted it at lower temperatures. These discrepancies were attributed to both secondary chemistry not included in the mechanism and the calibration technique required by the LIF detection method.

The DeSain PES was later refined by Estupiñán et al.^{10,11} through comparisons with subsequent measurements of HO₂ profiles using both C₃H₇ and C₃D₇ radicals. Building further upon the DeSain work, Huang et al.¹² used both a cleaner source of Cl-atoms and direct absorption experiments for improved OH-profile measurement. Further modifications to the DeSain PES resulted in better agreement between theory and experiment.

Although not part of the O₂ + propyl system, Fernandes et al.¹³ measured the OH concentration in Cl-initiated oxidation of cyclohexane at high pressure. They found that the OH profiles strongly suggest the presence of O₂ + QOOH chemistry.

In addition to Taatjes and co-workers, other groups have addressed the O₂ + propyl system from a purely computational perspective. Wijaya et al.,¹⁴ Green et al.,¹⁵ Merle et al.,¹⁶ Huynh et al.,¹⁷ Bozzelli and Chen,¹⁸ Zhang and Dibble,¹⁹ and Miyoshi²⁰ computed aspects of the potential energy surface using the compound CBS-QB3 method.²¹ Huynh et al. and Bozzelli and Chen used these electronic energies to compute temperature- and pressure-dependent rate coefficients using QRRK theory with a modified strong collision (MSC) model for collisional energy transfer, and Huynh et al. combined these results with a larger mechanism for propane oxidation. Although the QRRK/MSC method is less rigorous than the RRKM/ME method used in refs 4, 5, and 9–12, the Huynh et al. model was in good agreement with the experimental HO₂ profiles of Estupiñán et al. In addition to the O₂ + propyl PES, Bozzelli also used a CBS-Q-type method to compute the O₂ + 3-hydroperoxy-1-propyl PES. The corresponding temperature and pressure dependent rate coefficients were computed using QRRK/MSC. The present work improves upon this analysis by utilizing more accurate electronic structure calculations combined with a more rigorous RRKM/ME calculation, and by including additional QOOH isomers in the second O₂ addition reaction. Zhang and Dibble performed CCSD(T) benchmark calculations for ROO ↔ QOOH and ROO ↔ alkene + HO₂, including a detailed comparison of various tunneling models.²² Miyoshi²⁰ presented a systematic computational study on RO₂, QOOH, and O₂QOOH radicals and how the high-pressure limit rate coefficients change based upon substitution. Villano et al.²³ present a similar set of high-pressure rate rules for RO₂ dissociation, concerted elimination, and isomerization. Sharma et al.²⁴ computed the thermochemistry and rate coefficients for several intramolecular hydrogen migration reactions involving alkylperoxy and hydroperoxyalkylperoxy radicals (i.e., ROO ↔ QOOH and OOQOOH ↔ HOOQ'OOH reactions), including those on the C₃H₇O₂ and C₃H₇O₄ PES. The latter work highlighted the significance of the multidimensional nature of coupled hindered internal rotation in hydroperoxyalkylperoxy radicals.

The present work examines the role of O₂ + QOOH chemistry in low-temperature alkyl autoignition, employing ab initio transition-state theory based master-equation calculations to determine many of the key rate constants for the propane oxidation system. The propane system was selected as a model for study because it is the smallest hydrocarbon that exhibits negative temperature coefficient behavior, thereby simplifying the theoretical analysis. Furthermore, this system has been the subject of extensive experimental study.^{4,5,9–12} Such studies are continuing under the auspices of the Argonne-Sandia consortium on high pressure combustion chemistry.

The initial hydrogen abstractions from propane yield significant amounts of both *n*-propyl and isopropyl. The

O₂ + *n*-propyl and O₂ + isopropyl reactions yield three distinct C₃H₆OOH (QOOH) isomers. A key aspect of this study involves the computation of the potential energy surface, high-pressure limit rate coefficients, and pressure-dependent rate coefficients for the reaction of these three QOOH radicals with molecular oxygen using high-level computational quantum mechanics and RRKM/ME techniques. We also study the decomposition kinetics for some of the key C₃H₆O₃, C₃H₆O₂, and C₃H₅O₂ products arising from the O₂ + QOOH reactions. For completeness, we provide updated predictions for the O₂ + propyl radical kinetics employing higher level estimates for the stationary point energies. Finally, a new kinetic mechanism is developed to quantify the effect of O₂ + QOOH chemistry on chain-branching.

2. THEORY

2.1. Potential Energy Surfaces. Seventy-one stationary points were computed for the C₃H₆O₂, C₃H₇O₂, C₃H₆O₃, and C₃H₇O₄ potential energy surfaces. For each species and transition state, the ~3ⁿ possible conformers, where *n* is the number of torsional modes, were calculated using the CBS-QB3 method. The lowest energy conformer was selected, and this geometry was reoptimized using the B3LYP functional with the 6-311++G(d,p) basis set. For the species and transition states on the C₃H₆O₂ and C₃H₇O₂ potential energy surfaces, restricted QCISD(T)/cc-pVTZ and QCISD(T)/cc-pVQZ energies were calculated at the DFT geometries. The QCISD(T) complete basis set (CBS) limit was extrapolated from the triple and quadruple- ζ basis set calculations assuming an inverse power law:^{25,26}

$$E_{\text{CBS}}^{\text{QCI}} = E_{\text{QZ}}^{\text{QCI}} + (E_{\text{QZ}}^{\text{QCI}} - E_{\text{TZ}}^{\text{QCI}}) \frac{4^4}{5^4 - 4^4} \quad (\text{E1})$$

For the C₃H₆O₃ and C₃H₇O₄ potential energy surfaces, the QCISD(T)/cc-pVQZ calculations were computationally prohibitive. Instead, restricted QCISD(T)/cc-pVDZ and QCISD(T)/cc-pVTZ energies were calculated at the DFT geometries, and the CBS limit energy was estimated from extrapolations of the cc-pVDZ and cc-pVTZ results. The MP2 method was then used to correct for the difference in cc-pVDZ, cc-pVTZ and cc-pVTZ, cc-pVQZ based extrapolations yielding:²⁷

$$\begin{aligned} E_{\text{CBS}}^{\text{QCI}} = & E_{\text{TZ}}^{\text{QCI}} + (E_{\text{TZ}}^{\text{QCI}} - E_{\text{DZ}}^{\text{QCI}}) \frac{3^4}{4^4 - 3^4} \\ & + E_{\text{QZ}}^{\text{MP2}} + (E_{\text{QZ}}^{\text{MP2}} - E_{\text{TZ}}^{\text{MP2}}) \frac{4^4}{5^4 - 4^4} \\ & - E_{\text{TZ}}^{\text{MP2}} - (E_{\text{TZ}}^{\text{MP2}} - E_{\text{DZ}}^{\text{MP2}}) \frac{3^4}{4^4 - 3^4} \end{aligned} \quad (\text{E2})$$

The QCISD(T)/CBS enthalpies at 0 K, including the B3LYP/6-311++G(d,p) zero point energies, for the C₃H₇O₂, C₃H₇O₄, C₃H₆O₂, and C₃H₆O₃ potential energy surfaces are listed in Tables 1–8. Also included in these tables are the QCISD(T)/cc-pVQZ or QCISD(T)/cc-pVTZ T1 diagnostic for the equilibrium and saddle point geometries, which is a measure of the importance of multireference effects.²⁸ For closed shell species with a T1 diagnostic less than ~0.02, and for radicals with a T1 diagnostic less than ~0.03, the QCISD(T)/CBS energies are expected to be accurate to ~1 kcal/mol, and multireference calculations are unnecessary.²⁹

Second-order multireference perturbation theory (CASPT2)³⁰ was used to study the barrierless reactions. All DFT calculations were done using Gaussian03.³¹ All QCISD(T) and CASPT2 calculations were done using MOLPRO.³²

2.2. Variable Reaction Coordinate TST Calculations. As noted in the Introduction, the addition of molecular oxygen to an alkyl radical proceeds without an intrinsic barrier. These reactions are treated here with variable reaction coordinate transition-state theory (VRC-TST).^{7,33,34} In these VRC-TST calculations the degrees of freedom are separated into conserved and transitional modes. The conserved modes, which are the vibrational modes of the two fragments, were treated as harmonic vibrators employing the frequencies and geometries of the isolated fragments. The transitional modes, which are the coupled, anharmonic modes correlating with the relative orientation and separation of the two fragments, were treated via Monte Carlo integration of a classical phase space representation.

For the $\text{O}_2 + \text{QOOH}$ and $\text{C}_3\text{H}_6\text{O}_3$ decomposition reactions, the VRC-TST calculations were done using the computer code VaReCoF,³⁵ and the requisite transitional mode interaction energies were calculated on-the-fly using multireference second-order perturbation theory (CASPT2). For the $\text{O}_2 + \text{QOOH}$ reactions, a minimum active space of seven electrons in five orbitals (7e,5o) was chosen: six electrons in four orbitals for molecular oxygen and one electron in one orbital for the carbon-centered radical. For the $\text{C}_3\text{H}_6\text{O}_3$ decompositions the minimum active space was (6e,4o), which accounts for three electrons in two orbitals on each oxygen-centered product radical.³⁶

For these reactions, two sets of CASPT2/cc-pVDZ geometry optimizations were performed along the minimum energy path (MEP) from 1.5 to 5 Å. In one set, all of the modes were relaxed; in the other set, the conserved modes were held fixed at their isolated geometries, and only the transitional modes were optimized. The CASPT2/CBS energy was extrapolated from subsequent CASPT2/aug-cc-pVDZ and CASPT2/aug-cc-pVTZ calculations using a formula similar to eq E1. The difference in energy between the constrained and relaxed MEP was added to the CBS correction and used as a 1-D correction to the interaction potential.

For the $\text{O}_2 + n$ -propyl and $\text{O}_2 + \text{isopropyl}$ reactions, the analytic potential of DeSain⁴ was used for these VRC-TST calculations. Attempts to predict accurately the rate coefficients for these two reactions with direct CASPT2 VRC-TST calculations were hampered by the presence of relatively strong interactions between one of the O atoms and one of the H atoms. This interaction correlates with a strong coupling of the torsional modes of the fragments (considered as conserved modes) with the transitional modes. Neglecting this coupling, as currently required by the VaReCoF program, would lead to errors on the order of a factor of 2. Thus, for these two reactions we simply chose to use the prior model potential results, which accurately reproduce the available experimental data.

2.3. Master Equation Calculations. The time-dependent master equation was solved using the computer code Variflex.³⁷ A single-exponential down model was used to represent the collisional energy transfer probability. To account for the weak temperature- and size-dependence of the energy transfer parameter, $\langle \Delta E_{\text{down}} \rangle$, a value of $200 (T/300)^{0.85} \text{ cm}^{-1}$ was used for the $\text{C}_3\text{H}_7\text{O}_2$ PES, and $300 (T/300)^{0.85} \text{ cm}^{-1}$ was used for the $\text{C}_3\text{H}_7\text{O}_4$ PES. The collision frequency was estimated using a Lennard-Jones (LJ) model, with LJ parameters of $\sigma = 4.36 \text{ Å}$ and $\epsilon = 292 \text{ cm}^{-1}$ for $\text{C}_3\text{H}_7\text{O}_2$, $\sigma = 4.46 \text{ Å}$ and $\epsilon = 336 \text{ cm}^{-1}$ for

$\text{C}_3\text{H}_6\text{O}_3$, $\sigma = 4.20 \text{ Å}$ and $\epsilon = 351 \text{ cm}^{-1}$ for $\text{C}_3\text{H}_7\text{O}_4$. The LJ parameters for the wells were based on group additivity of the functional groups.³⁸ The He bath gas LJ-parameters, $\sigma = 2.55 \text{ Å}$ and $\epsilon = 6.96 \text{ cm}^{-1}$, were taken from literature values.³⁹ All master equation calculations were performed at temperatures between 400 and 1500 K and pressures between 0.01 and 100 atm of He.

The tight transition states were treated with conventional transition-state theory employing rigid-rotor harmonic oscillator assumptions for most modes. However, the torsional modes for each species and transition state were treated as one-dimensional hindered internal rotors. The barriers for internal rotation were calculated by a relaxed scan at the B3LYP/6-31+G(d,p) level. The resulting potential was fit to a Fourier series. To reduce the ambiguity regarding low-frequency vibrations and the corresponding torsional modes, the projection of the B3LYP/6-311++G(d,p) force-constant matrix was removed along the vectors corresponding to changing each dihedral angle while holding the other internal coordinates fixed. This matrix was then diagonalized, which separated the rigid-rotor harmonic-oscillator frequencies from the torsional modes.²⁴ These frequencies were then scaled by 0.99. A Pitzer-Gwinn-like⁴⁰ approximation was made within Variflex for the hindered rotor partition function. Tunneling was included for all transition states by use of an asymmetric Eckart approximation.⁴¹

As detailed by Sharma et al.,²⁴ hindered internal rotation in hydroperoxyalkylperoxy radicals cannot be described accurately by independent 1D rotors, due to variations in the torsional barriers that arise from the presence or absence of hydrogen bonding interactions. The lowest energy conformer is a quasi-cyclic structure characterized by hydrogen bonding between the oxygen-centered radical and the OOH moiety; this geometry is roughly 2 kcal/mol more stable than a straight-chain conformer. 1D hindered-rotor barriers obtained from this initial cyclic geometry are quite high, with barriers in the 5–8 kcal/mol range. In contrast, hindered-rotor barriers obtained from the straight-chain conformer are roughly half as large, owing to the absence of internal hydrogen bonding. The lowest-energy conformer is confined to a narrow well by the hydrogen bonding. Once it has sufficient energy to break this bond, it can sample a significantly larger conformational space, and the density of states will increase dramatically at energies greater than the hydrogen bond strength.

A combination of separable 1D rotors cannot reproduce this kink in the density of states. If the rotational barriers obtained from the lowest energy conformer are used, then the density of states will be underestimated at higher energies. Consequently, the microcanonical rate constant will be overpredicted. In contrast, if the barriers from the straight-chain conformer are used, then the density of states is overpredicted, because the calculation is sampling from more states at lower energies than should be allowed. Accurate treatment of this effect requires a multidimensional rotor model.

Incorporating such a model into our RRKM code is beyond the scope of this paper. Instead, we continue to assume that the rotors are 1D. As a crude approximation, we have chosen to split the difference: for a hydroperoxyalkylperoxy radical of the form $\text{HO}_4\text{O}_3\text{C}_3\text{C}_2\text{C}_1\text{O}_2\text{O}_1^*$, the rotational potentials for the $\text{HO}_4\text{O}_3\text{C}_3$, $\text{O}_4\text{O}_3\text{C}_3\text{C}_2$, and $\text{C}_2\text{C}_1\text{O}_2\text{O}_1^*$ dihedral angles are taken from the quasi-cyclic structure, and the remaining rotational potentials for the $\text{O}_3\text{C}_3\text{C}_2\text{C}_1$ and $\text{C}_3\text{C}_2\text{C}_1\text{O}_2$ dihedral angles are taken from the straight chain. Section 3.5 analyzes the

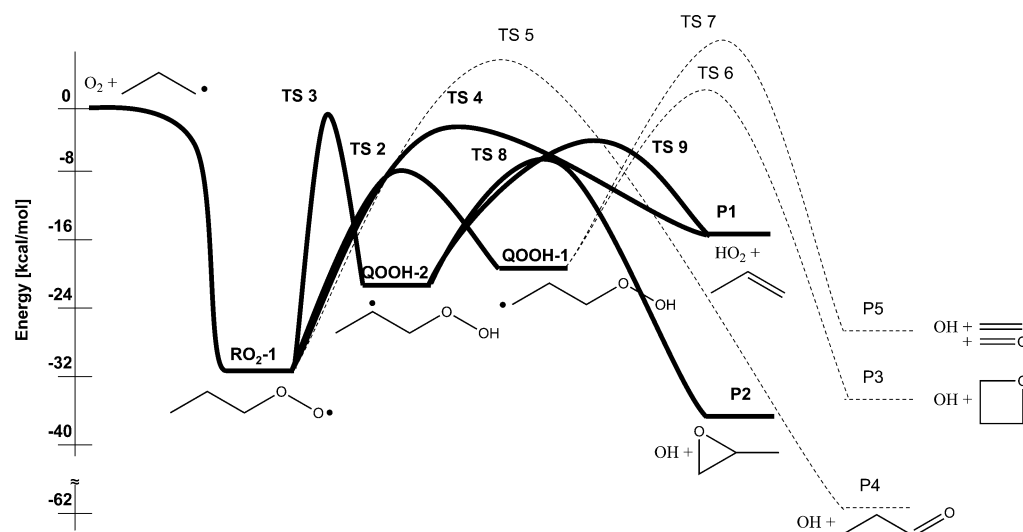


Figure 2. $O_2 + n$ -propyl potential energy surface. The channels shown with dashed lines are not included in the RRKM/ME calculations.

uncertainty in the phenomenological rate coefficients associated with this assumption.

3. RESULTS AND DISCUSSION

3.1. Potential Energy Surfaces. **3.1.1. $O_2 + n$ -Propyl Potential Energy Surface.** The $O_2 + n$ -propyl zero-point corrected PES is shown in Figure 2. The relative energies for the minima and saddle points on this PES are listed in Tables 1 and 2, respectively. The most stable intermediate is the initial adduct, n -propylperoxy (RO_2 -1). The lowest reaction barrier from this well is isomerization to 3-hydroperoxyl-1-propyl (QOOH-1), TS2, which proceeds via a 1,5p H-transfer. The 1,5p notation refers to the position of the heavy atoms involved in the transition state and the type of radical produced (e.g., primary, secondary, or tertiary); thus, a 1,5p H-transfer refers to a six-member ring (O–O–C–C–C–H) transition state that yields a primary radical. The barrier for isomerization is 8.5 kcal/mol below the reactants in energy; consequently, some of the initial $O_2 + n$ -propyl adduct (RO_2 -1) will go directly to form QOOH-1. All decomposition barriers from QOOH-1 are above the reactants in energy, so this species will rapidly equilibrate with RO_2 -1 instead of decomposing.

The next lowest barrier from RO_2 -1 is that for the concerted HO_2 elimination, TS4. This barrier is 2.7 kcal/mol below the reactants, thereby facilitating the formally direct formation of $HO_2 +$ propene from $O_2 + n$ -propyl.

The other $C_3H_7O_2$ isomer, 3-hydroperoxyl-2-propyl (QOOH-2), is more stable than QOOH-1 (as it is a secondary radical). However, its formation from RO_2 -1 proceeds via a 1,4s H-transfer, which has a barrier, TS3, that is almost isoenergetic with the reactants. QOOH-2 can decompose to $OH +$ propylene oxide, via TS8, and $HO_2 +$ propene, via TS9. Because these decomposition barriers are several kcal/mol below the preceding isomerization barrier, and the QOOH-2 well is shallow, it is expected that most of the energetically excited QOOH-2[†] adduct will decompose rather than undergo collisional stabilization.

3.1.2. $O_2 +$ Isopropyl Potential Energy Surface. The $O_2 +$ isopropyl PES is shown in Figure 3, with the corresponding energies for the minima and saddle points provided in Tables 3 and 4, respectively. The initial adduct is isopropylperoxy, RO_2 -2. Due to symmetry, there is only one QOOH isomer for



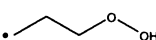
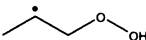

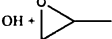
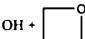
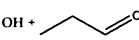
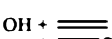
RO_2 -2, 2-hydroperoxyl-1-propyl (QOOH-3). Unlike the RO_2 -1 isomerizations, the barrier for isomerization from RO_2 -2 to QOOH-3 is above the reactants in energy. This result is consistent with results for $O_2 +$ ethyl.⁴ Isomerization from CH_3CH_2OO to CH_3CH_2OOH , because both involve a 1,4p H-transfer. In contrast, although isomerization from RO_2 -1 to QOOH-2 also involves a five-member ring, the product is a secondary radical, so the barrier relative to reactants is lower (in this case by ~ 1.4 kcal/mol).

The only barrier from RO_2 -2 that is below the reactants in energy is the concerted HO_2 elimination, TS12. Consequently, the dominant formally direct bimolecular product channel is expected to be $HO_2 +$ propene. Reaction via TS11 will lead primarily to $OH +$ propylene oxide at reasonable pressures, but this channel is much slower than $HO_2 +$ propene production.

Tables 1–4 also provide previous characterizations of the $C_3H_7O_2$ potential energy surfaces. The present energies are expected to be more accurate due to their use of larger basis sets, particularly in the QCISD(T) part of the calculations. In general, the agreement is quite good, with typical differences of 2–3 kcal/mol. It is interesting to compare the present values with the results derived from DeSain et al. and Huang et al.,^{4,9–12} listed in the column labeled DeSain. The results of DeSain et al.^{4,9–11} were obtained by modifying specific values on the PES to improve the agreement between predicted and measured yields for OH and HO_2 . With the one exception of TS11 in Huang et al.,¹² in every case the modifications made to the original PES result in new values that are in closer agreement with the present work. This improving agreement suggests a convergence between experimental and computational results. Although we believe our values are the best ab initio calculations published so far, much higher-level calculations are expected to be published soon by Liang and Allen.⁴² There is generally good agreement among the calculations and values inferred from experiment on all the stationary points. A prominent exception is TS3, which lies near a conical intersection,⁴² where for example our value in Table 2 differs by more than 2 kcal/mol from prior work. Small but significant discrepancies remain for TS4, TS8, TS18, TS19, and TS22; further work on these transition states using even higher levels of theory would be helpful.

3.1.3. $O_2 +$ 3-Hydroperoxyl-1-propyl (QOOH-1) Potential Energy Surface. The $O_2 +$ QOOH-1 PES is shown in Figure 4,

Table 1. Species for *n*-Propyl + O₂ Potential Energy Surface

#	Species Name	Structure	Relative Energy ^a			T1 diagnostic
			Present work	DeSain ^b	CBS-Q ^c	
R1+O ₂	<i>n</i> -propyl + O ₂		0.0	0.0	0.0	0.010, 0.007
RO ₂ -1	<i>n</i> -propylperoxy		-33.3	-34.9 ^d -33.9 ^e	-34.8 ^f -35.3 ^g -34.8 ^h	0.029
QOOH-1	3-hydroperoxyl-1-propyl		-18.1	-19.8 ^d	-18.9 ^f -18.7 ^g -17.4 ^j -17.2 ^k	0.012
QOOH-2	3-hydroperoxyl-2-propyl		-20.4	-21.6 ^d	-21.4 ^f -21.2 ^g -19.4 ^k	0.013
P1	propene + HO ₂		-16.5		-15.1 ^j -16.5 ^k	0.010, 0.037
P2	propylene oxide + OH		-38.6			0.011, 0.007
P3	oxetane + OH ^l		-35.1		-34.5 ⁱ	0.010, 0.007
P4	propanal + OH ^l		-61.5			0.014, 0.007
P5	ethene + formaldehyde + OH ^l		-31.1			0.011, 0.016, 0.007

^aAll energies are 0 K E_0 , relative to O₂ + *n*-propyl, in kcal/mol. ^bThe column DeSain refers to the original PES in ref 9 and all subsequent modifications; ^cThe column CBS-Q refers to literature values obtained using CBS-QB3 or similar methods. ^dDeSain.⁹ ^eHuang.¹² ^fMerle.¹⁶ ^gBozzelli.¹⁸ ^hHuynh.¹⁷ ⁱWijaya.¹⁴ ^jZhang.¹⁹ ^kRefers to the CCSD(T)/aug-cc-pVTZ results in Zhang and Dibble.²² ^lProducts P3, P4, and P5 are not included in the RRKM/ME calculations.

with the energies for the minima and saddle points provided in Tables 5 and 6, respectively. The initial adduct is 3-hydroperoxyl-*n*-propylperoxy, Well-1. This oxygen-centered radical can abstract an H-atom from any of the three carbon atoms. However, only the abstraction from the middle carbon, via TS17, leads to a stable isomer. The result is 1,3-dihydroperoxyl-2-propyl, Well-4. If an H-atom is abstracted from either of the other two carbons, the result is an α -hydroperoxyalkyl radical, which is at most metastable. Indeed, at the level of theory used in the present work, no stable α -hydroperoxyalkyl geometries could be determined, which is consistent with previous literature results.^{24,43} Thus, we have replaced the α -hydroperoxyalkyl radicals with their dissociative products, OH + keto-hydroperoxides. The H-Abstraction from C1 in Well-1 involves a four-member ring transition state, TS 20, which is energetically prohibitive and so is not illustrated. Abstraction from C3, in contrast, occurs via a six-member ring transition state, TS19, that is roughly 12 kcal/mol below the reactants in energy. Importantly, this reaction is the main chain-branching mechanism in low-temperature autoignition.

The decomposition of the resulting 2-formylethyl hydroperoxide, P9a, leads to OH + 2-formylethoxy. This O–O bond scission reaction is the reverse of a radical–radical reaction, and

as such it has no barrier beyond the intrinsic endothermicity of the reaction. Furthermore, the energy of the three products, OH + OH + 2-formylethoxy, is still ~12 kcal/mol below the energy of the O₂ + QOOH-1 reactants. It is conceivable, therefore, that some if not all of the formally direct channel O₂ + QOOH-1 → OH + 2-formylethyl hydroperoxide would in fact be observed as O₂ + QOOH-1 → OH + OH + 2-formylethoxy.

Unfortunately, it is difficult to predict a priori the fraction of the energetically excited C₃H₆O₃[‡] product that will directly decompose leading to immediate appearance of OH + OH + RO. Some of the excess energy from its formation via O₂ + QOOH-1 will be lost to the internal vibrational energy of the OH coproduct and to the rotational and translational energies of the fragments. Accurate predictions would require detailed dynamical simulations of the dissociation process from Well-1 and of the collision induced evolution of the energy distribution in C₃H₆O₄[‡]. The result would likely be a complex function of temperature and pressure. Such calculations were deemed beyond the scope of the present work.

In the kinetic model described in section 3.4, we assume for simplicity that all of the directly formed keto-hydroperoxide,

$\text{C}_3\text{H}_6\text{O}_3^\ddagger$, retains enough internal energy to decompose. In other words, the reaction $\text{O}_2 + \text{QOOH-1} \rightarrow \text{OH} + 2\text{-formylethyl hydroperoxide}$ is replaced by $\text{O}_2 + \text{QOOH-1} \rightarrow \text{OH} + \text{OH} + 2\text{-formyl ethoxy}$. Note that there is a competing pathway to the same products via a sequence of thermal reactions, which can be more important than the chemically activated reactions at high P and low T . In contrast, the thermally activated dissociation of

Table 2. Transition States for n -Propyl + O_2 Potential Energy Surface^a

no.	reactions	relative energy ^a			T1 diagnostic
		present work	DeSain ^b	CBS-Q ^c	
TS 1	$\text{R1} + \text{O}_2 \leftrightarrow \text{RO}_2\text{-1}$	barrierless			
TS 2	$\text{RO}_2\text{-1} \leftrightarrow \text{QOOH-1}$	-8.5	-11.2 ^d	-10.9 ^g -11.9 ^h -9.5 ⁱ -9.5 ^k -8.6 ^l	0.025
TS 3	$\text{RO}_2\text{-1} \leftrightarrow \text{QOOH-2}$	-0.2	-2.6 ^d -2.1 ^e -2.1 ^f	-2.7 ^g -3.7 ^h -1.2 ⁱ -0.1 ^l	0.027
TS 4	$\text{RO}_2\text{-1} \leftrightarrow \text{P1}$	-2.7	-5.2 ^d -3.8 ^e -3.8 ^f	-3.9 ^g -5.4 ^h -2.4 ⁱ -2.4 ^k -3.2 ^l	0.035
TS 5	$\text{RO}_2\text{-1} \leftrightarrow \text{P4}$	8.1			0.020
TS 6	$\text{QOOH-1} \leftrightarrow \text{P3}$	2.9		3.4 ^j	0.022
TS 7	$\text{QOOH-1} \leftrightarrow \text{P5}$	9.0			0.020
TS 8	$\text{QOOH-2} \leftrightarrow \text{P2}$	-3.2	-3.4 ^d	-6.1 ^g -5.8 ^h	0.030
TS 9	$\text{QOOH-2} \leftrightarrow \text{P1}$	-8.1	-6.5 ^d	-9.3 ^g -6.4 ^h	0.019

^aAll energies are 0 K E_0 , relative to $\text{O}_2 + n$ -propyl, in kcal/mol. ^bThe column DeSain refers to the original PES in ref 9 and all subsequent modifications. ^cThe column CBS-Q refers to literature values obtained using CBS-QB3 or similar methods. ^dDeSain.⁹ ^eDeSain.⁴ ^fHuang.¹² ^gMerle.¹⁶ ^hBozzelli.¹⁸ ⁱHuynh.¹⁷ ^jWijaya.¹⁴ ^kZhang.¹⁹ ^lRefers to the CCSD(T)/aug-cc-pVTZ results in Zhang and Dibble.²² ^mTransition states TS 5, TS 6, and TS 7 are not included in the RRKM/ME calculations.

Well-1 is assumed to proceed to $\text{OH} + 2\text{-formylethyl hydroperoxide}$ and not to $\text{OH} + \text{OH} + 2\text{-formylethoxy}$. Because the exothermicity is significantly smaller, the reactions via Well-4 are assumed to proceed to $\text{OH} + \text{oxiranylmethyl hydroperoxide}$, not directly yielding a second OH.

The other dissociation channel available to Well-1 is the concerted HO_2 elimination via TS18, which is 3.5 kcal/mol below the reactants in energy. The barrier for this channel is almost 9 kcal/mol higher than the 1,5s H-transfer (chain branching) barrier, so the HO_2 yield is expected to be considerably smaller. However, the 1,5s H-transfer transition state has a greater loss of entropy relative to Well-1 than the concerted elimination transition state, so the $\text{HO}_2 + \text{allyl hydroperoxide}$ channel does become competitive at higher temperatures.

3.1.4. $\text{O}_2 + 3\text{-Hydroperoxyl-2-propyl (QOOH-2)}$ and $\text{O}_2 + 2\text{-Hydroperoxyl-1-propyl (QOOH-3)}$ Potential Energy Surface. The $\text{O}_2 + \text{QOOH-2}$ and $\text{O}_2 + \text{QOOH-3}$ potential energy surface is shown in Figure 5, with the corresponding energies for the minima and saddle points provided in Tables 7 and 8, respectively. The initial adduct for $\text{O}_2 + \text{QOOH-2}$ is 1-methyl-2-hydroperoxylethylperoxy, Well-2; the initial adduct for $\text{O}_2 + \text{QOOH-3}$ is 2-hydroperoxyl- n -propylperoxy, Well-3. These two adducts can isomerize rapidly via TS25, a seven-member ring transition state in which the hydrogen atom is passed back and forth between the two peroxy groups. There is only one six-member ring transition state on this surface, the isomerization from Well-3 to 2,3-dihydroperoxy- n -propyl, Well-5, via TS31. The remaining H-abstraction reactions all proceed via five-member ring transition states.

For Well-2 and Well-3, there are multiple decomposition channels with similar barrier heights. In particular, TS27–29, and TS34–36 barriers range from -5.7 to -2.6 kcal/mol relative to $\text{O}_2 + \text{QOOH-2}$. Thus, in contrast to the $\text{O}_2 + \text{QOOH-1}$ PES, there is no single channel that clearly dominates. Starting from Well-2, the dominant reactions are isomerization to Well-3 and decomposition back to $\text{O}_2 + \text{QOOH-2}$. The dominant bimolecular production channels are $\text{OH} + 1\text{-formylethyl hydroperoxide (P12a)}$, followed by $\text{HO}_2 + \text{allyl hydroperoxide (P7a)}$ and $\text{HO}_2 + \text{propen-1-yl hydroperoxide (P10a)}$. Starting from Well-3, the dominant reactions are isomerization to Well-2 and Well-5 and decomposition back to $\text{O}_2 + \text{QOOH-3}$. The dominant bimolecular product channels are $\text{OH} + \text{acetylmethyl hydroperoxide (P13a)}$ and $\text{HO}_2 + \text{propen-2-yl hydroperoxide}$.

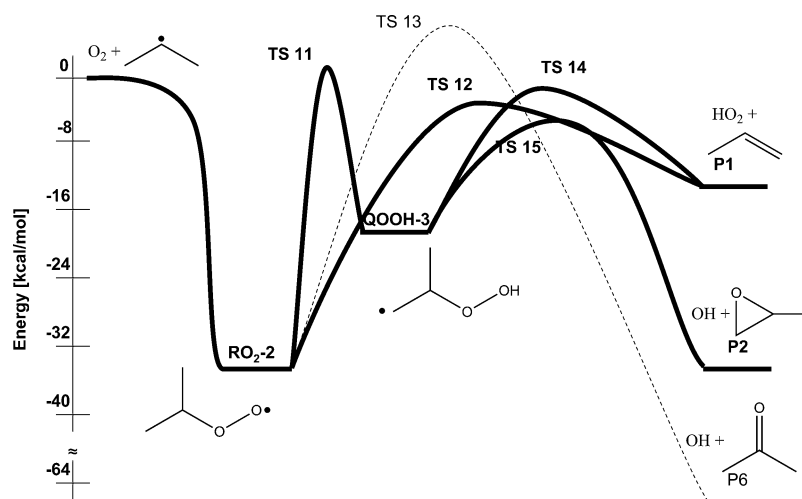
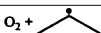
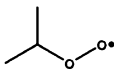
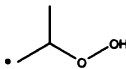
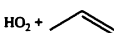
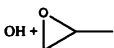
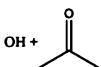


Figure 3. $\text{O}_2 + \text{isopropyl}$ potential energy surface. The channel shown with a dashed line is not included in the RRKM/ME calculations.

Table 3. Species for Isopropyl + O₂ Potential Energy Surface^a

#	Species Name	Structure	Relative energy ^a			T1 diagnostic
			Present work	DeSain ^b	CBS-Q ^c	
R2 + O ₂	i-propyl + O ₂		0.0	0.0	0.0	0.011, 0.007
RO ₂ -2	i-propylperoxy		-34.8	-36.8 ^d -34.8 ^e -34.8 ^f	-36.2 ^g	0.029
QOOH-3	2-hydroperoxyl- 1-propyl		-18.0	-20.2 ^d		0.013
P1	propene + HO ₂		-13.4			0.010, 0.037
P2	propylene oxide + OH		-35.5			0.011, 0.007
P6	acetone + OH ^h		-65.5			0.014, 0.007

^aAll energies are 0 K E_0 , relative to O₂ + isopropyl, in kcal/mol. ^bThe column DeSain refers to the original PES in ref 9 and all subsequent modifications. ^cThe column CBS-Q refers to literature values obtained using CBS-QB3 or similar methods. ^dDeSain.⁹ ^eEstupiñán.^{10,11} ^fHuang.¹² ^gHuynh.¹⁷ ^hProduct P6 is not included in the RRKM/ME calculations.

Table 4. Transition States for Isopropyl + O₂ Potential Energy Surface

no	reactions	relative energy ^a			T1 diagnostic
		present work	DeSain ^b	CBS-Q ^c	
TS 10	R2 + O ₂ ↔ RO ₂ -2	barrierless			
TS 11	RO ₂ -2 ↔ QOOH-3	1.2	-1.4 ^d -0.2 ^e -1.7 ^g	1.6 ^h	0.029
TS 12	RO ₂ -2 ↔ P1	-4.2	-7.0 ^d -4.7 ^e -6.0 ^f -5.0 ^g	-3.6 ^h	0.035
TS 13	RO ₂ -2 ↔ P6	5.5			0.019
TS 14	QOOH-3 ↔ P1	-1.3	-1.9 ^d		0.020
TS 15	QOOH-3 ↔ P2	-5.6	-4.9 ^d		0.020

^aAll energies are 0 K E_0 , relative to O₂ + isopropyl, in kcal/mol. ^bThe column DeSain refers to the original PES in ref 9 and all subsequent modifications. ^cThe column CBS-Q refers to literature values obtained using CBS-QB3 or similar methods. ^dDeSain.⁹ ^eDeSain.⁴ ^fEstupiñán.^{10,11} ^gHuang.¹² ^hHuynh.¹⁷ ⁱTransition state TS 13 is not included in the RRKM/ME calculations.

3.1.5. C₃H₆O₃ and C₃H₆O₂ Decomposition Potential Energy Surfaces. As described in sections 3.1.3 and 3.1.4, the O₂ + QOOH reaction yields a mixture of HO₂ + alkenyl hydroperoxides and OH + keto-hydroperoxides. These peroxide species are less stable than the corresponding alkene or ketone, due to the weakness of the RO–OH bond. Importantly, the breaking of this bond results in a chain branching reaction. To quantify the chain branching effect of these decomposition reactions, the energies of the various decomposition products and the transition states leading to them were computed. These energies are provided in Tables 5–9.

The decomposition of allyl hydroperoxide to OH + allyloxy is nearly 30 kcal/mol above O₂ + QOOH-1 in energy.

Therefore, the formally direct channel O₂ + QOOH-1 → HO₂ + OH + allyloxy is not feasible. Instead, the chain branching sequence must first pass through the stabilized allyl hydroperoxide intermediate: O₂ + QOOH-1 → HO₂ + allyl-hydroperoxide, followed by allyl hydroperoxide → OH + allyloxy. The thermal dissociation of allyl hydroperoxide and subsequent decomposition of allyloxy was described in detail in Goldsmith et al.,⁴⁴ and those results are included here.

The other two alkenyl hydroperoxides, 1-propenyl hydroperoxide and 2-propenyl hydroperoxide (hereafter referred to jointly as propenyl hydroperoxide), are markedly different. The resulting C₃H₅O₂ isomers, propen-1-oxy and propen-2-oxy (hereafter referred to jointly as propenoxy), are resonantly stabilized radicals. Owing to the delocalization of the unpaired electron along the C=C–O* bond (akin to vinoxy), these species are nearly 30 kcal/mol more stable than allyloxy. Consequently, these product channels are nearly isoenergetic with the O₂ + QOOH-2 reactants. Nonetheless we continue to assume that these chain-branching sequences occur through the stabilized hydroperoxide intermediate: O₂ + QOOH-2 → HO₂ + propenyl hydroperoxide, followed by thermalized propenyl hydroperoxide → OH + propenoxy.

Importantly, even though these sequences are nominally chain branching, the effect on ignition acceleration is muted. Two of the three radicals produced (HO₂ and propenoxy) are significantly less reactive than other radical species. HO₂ and resonantly stabilized radicals tend to react primarily with other radicals. As a consequence, this reaction sequence behaves more like a chain propagating sequence, converting QOOH-2 to OH.

For the three main keto-hydroperoxides, the OH + OH + keto-oxy radical products are below the O₂ + QOOH reactants in energy: –12 kcal/mol for O₂ + QOOH-1, and –20 kcal/mol for O₂ + QOOH-2. The resulting keto-oxy radicals are themselves not particularly stable, and they will undergo rapid β-scission. Even though the barriers for the β-scission reactions

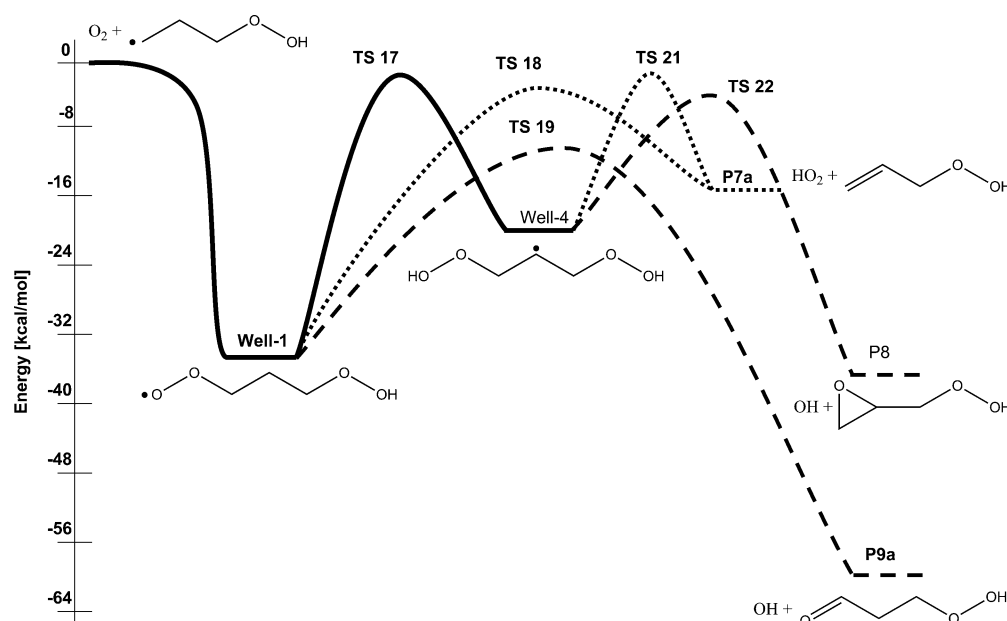


Figure 4. $\text{O}_2 + 3\text{-Hydroperoxyl-1-propyl (QOOH-1)}$ potential energy surface. The solid lines represent the entrance and isomerization channels; the dashed lines represent the $\text{OH} + \text{keto-hydroperoxide}$ product channels; the dotted lines represent the $\text{HO}_2 + \text{alkenyl hydroperoxides}$ product channels.

are below the $\text{O}_2 + \text{QOOH}$ energy reference, we do not assume the entire process can be modeled in a single step.

Another possible product from any of the $\text{O}_2 + \text{QOOH}$ reactions is oxiranylmethyl hydroperoxide. Unlike the keto-hydroperoxides, the decomposition products, $\text{OH} + \text{oxiranylmethoxy}$, are above the $\text{O}_2 + \text{QOOH}$ reactants in energy. The $\text{OH} + \text{oxiranylmethyl hydroperoxide}$ channel is a minor channel in $\text{O}_2 + \text{QOOH-2}$ and $\text{O}_2 + \text{QOOH-3}$. Therefore, the $\text{O}-\text{O}$ dissociation of oxiranylmethyl hydroperoxide was not computed explicitly. Instead, the rate coefficient for this reaction was taken from the decomposition of acetylmethyl hydroperoxide, because these two reactions have similar endothermicity.

3.2. High Pressure Limit Rate Constants. The computed high-pressure limit rate coefficients are shown in Figure 6 and 7 for a selected set of reactions. A complete set of modified Arrhenius fits for these high pressure rate coefficients are provided in Table 9. These fits reproduce the computed $k_\infty(T)$ to within 10% from 400 to 1500 K.

For $\text{O}_2 + \text{propyl radicals}$, a previously developed analytic potential was used for the barrierless entrance channel in the VRC-TST calculations; the force field for the transitional modes was assumed to decay exponentially with separation, and the corresponding force constants were adjusted to reproduce experimental high-pressure rate coefficients.⁴ Figure 6a,b shows that the high-pressure limit rate constant is within a factor of 2 of the values provided by Baulch et al.⁴⁵ for $\text{O}_2 + n\text{-propyl}$ and $\text{O}_2 + \text{isopropyl}$, respectively. The present rates are also within a factor of 2 of the recently estimated high-pressure rates in Huynh¹⁷ and Miyoshi.²⁰ For the $\text{O}_2 + \text{QOOH}$ reactions, shown in Figure 7a, there are no previous literature values for the high-pressure limit.

Also provided in Table 9 are recent literature values for the high-pressure limit rate coefficients for $\text{RO}_2 \rightarrow \text{QOOH}$ isomerization. The present predictions are within a factor of 3 of the rates in Huynh et al.,¹⁷ Sharma et al.,²⁴ Miyoshi,²⁰ Zhang and Dibble,²² and Villano et al.²³ which is reasonably satisfactory, considering the variety of methods used for estimating

the electronic energies, the hindered rotor partition functions, and tunneling corrections.

The high-pressure limit rate coefficients for keto-hydroperoxide decomposition are shown in Figure 7b. The high-pressure limit rate coefficient for the decomposition of allyl hydroperoxide ($\text{P7a} \rightarrow \text{P7b}$) was taken from Goldsmith et al.⁴⁴ The high-pressure limit rate coefficients for the decomposition of propenyl hydroperoxide ($\text{P10a} \rightarrow \text{P10b}$ and $\text{P11a} \rightarrow \text{P11b}$) were not computed; instead, the reverse rate coefficients were set equal to the rate coefficient for allyloxy + $\text{OH} \rightarrow \text{allyl hydroperoxide}$, which is reproduced in Figure 7b. As noted in section 3.1.5, because the propenoxy radicals are resonantly stabilized, the activation energies for the decomposition of 1-propenyl hydroperoxide and 2-propenyl hydroperoxide are considerably lower than for allyl hydroperoxide.

3.3. Pressure Dependent Rate Coefficients. The complete set of rate coefficients for the computed $\text{O}_2 + \text{C}_3\text{H}_7$ and $\text{O}_2 + \text{C}_3\text{H}_7\text{O}_2$ reactions, as well as the $\text{C}_3\text{H}_7\text{O}_2$, $\text{C}_3\text{H}_7\text{O}_4$, $\text{C}_3\text{H}_6\text{O}_3$, and $\text{C}_3\text{H}_6\text{O}_2$ decomposition reactions are provided in the Supporting Information in a CHEMKIN-compatible PLOG format, with modified Arrhenius parameters at 0.01, 0.1, 1, 10, and 100 atm.

3.3.1. $\text{O}_2 + n\text{-Propyl}$. The results of the master equation calculations for $\text{O}_2 + n\text{-propyl}$ are summarized in Figure 8. As illustrated in Figure 2, only the reaction channels that are below the reactants in energy are included. For simplicity, the discussion will be limited to the results at 1 atm (for other pressures, see the Supporting Information). At this pressure, the dominant product channel is $\text{RO}_2\text{-1}$. The rate constant for $\text{HO}_2 + \text{propene}$ and QOOH-1 are 3 orders of magnitude smaller at 400 K. As the temperature increases, the rate coefficient for $\text{RO}_2\text{-1}$ stabilization decreases, and the chemically activated rate coefficients increase; thus, by ~ 900 K, the rate constant for $\text{HO}_2 + \text{propene}$ is within an order of magnitude of the $\text{RO}_2\text{-1}$ stabilization rate constant. The rate constant for the formally direct $\text{O}_2 + n\text{-propyl} \rightarrow \text{OH} + \text{propylene oxide}$ reaction is generally a factor of 10 smaller than that for $\text{HO}_2 +$

Table 5. Species for O₂ + 3-Hydroperoxyl-1-propyl (QOOH 1) Potential Energy Surface

#	Species Name	Structure	Relative energy ^a		T1 diagnostic
			Present Work	CBS-Q ^b	
QOOH-1	3-hydroperoxyl-1-propyl + O ₂		0.0	0.0	0.012,
Well-1	3-hydroperoxyl-n-propylperoxy		-33.9	-34.7 ^c	0.007
Well-4	1,3-dihydroperoxyl-2-propyl ^d		-21.3	-22.6 ^c	0.026
P7a	allylhydroperoxide + HO ₂		-15.5	-14.3 ^c	0.012,
P7b	Allyloxy + OH + HO ₂		27.7		0.037
P8a	oxiranyl-methylhydroperoxide + OH		-38.7	-36.8 ^c	0.020,
P8b	Oxiranyl-methoxy + OH + OH		6.2		0.006,
P9a	2-formyl-ethylhydroperoxide + OH		-61.0	-60.4 ^c	0.018,
P9b	2-formyl-ethoxy + OH + OH		-17.2		0.006

^aAll energies are 0 K E_0 , relative to O₂ + QOOH-1, in kcal/mol. ^bThe column CBS-Q refers to literature values obtained using CBS-QB3. ^cBozzelli.¹⁸ ^dWell-4 is not included in the RRKM/ME calculations for this PES.

Table 6. Transition States for 3-Hydroperoxyl-1-propyl (QOOH 1) + O₂ Potential Energy Surface

no.	reactions	relative energy ^a		T1 diagnostic
		present work	CBS-Q ^b	
TS 16	QOOH-1 + O ₂ ↔ Well-1	barrierless		
TS 17	Well-1 ↔ Well-4	-0.8	-1.9 ^c	0.027
TS 18	Well-1 ↔ P7a	-3.6	-7.5 ^c	0.031
TS 19	Well-1 ↔ P9a	-12.3	-16.1 ^c	0.021
TS 20	Well-1 ↔ P9a	7.4		0.018
TS 21	Well-4 ↔ P7a	-5.1	-6.8 ^c	0.020
TS 22	Well-4 ↔ P8a	-4.6	-8.4 ^c	0.015

^aAll energies are 0 K E_0 , relative to O₂ + QOOH-1, in kcal/mol. ^bThe column CBS-Q refers to literature values obtained using CBS-QB3. ^cBozzelli.¹⁸ ^dTransition state TS 22 is not included in the RRKM/ME calculations.

propene at this pressure; nonetheless, this reaction is the dominant source of OH radicals in the first few microseconds after the reaction begins in Taatjes's experiments.^{4,5,9–12} The rate coefficient for O₂ + *n*-propyl → QOOH-2 is 4–5 orders of magnitude smaller than the rate coefficient for O₂ + *n*-propyl → RO₂-1.

The behavior is qualitatively similar at different pressures. At 10 atm, more RO₂-1 is stabilized, and the rate constants for the chemically activated channels are smaller (between a factor of 2 and an order of magnitude, depending upon the channel and the temperature). At 0.1 atm, in contrast, less RO₂-1 is stabilized, and the rate constants for the chemically activated channels are proportionally larger.

The phenomenological rate coefficients for O₂ + *n*-propyl → products are characterized by four chemically significant eigenvalues. The largest of the chemically significant eigenvalues, λ_4 , approaches the continuum of energy transfer eigenvalues around 950 K at 1 atm, with the crossover temperature increasing as the pressure increases. Beyond this temperature RO₂-1 and QOOH-1 will equilibrate on a shorter time scale than that of internal energy transfer. Consequently, above 950 K RO₂-1 and QOOH-1 are no longer distinct chemical species. Instead, the O₂ + *n*-propyl reaction forms an admixture of the two, which we call ROO' for simplicity. Of course, this merging of two species into one new species presents a challenge for modeling O₂ + QOOH chemistry.

For such modeling purposes, we wish to retain two separate rate coefficients even at temperatures where only the one effective rate constant for formation of ROO' exists. We accomplish

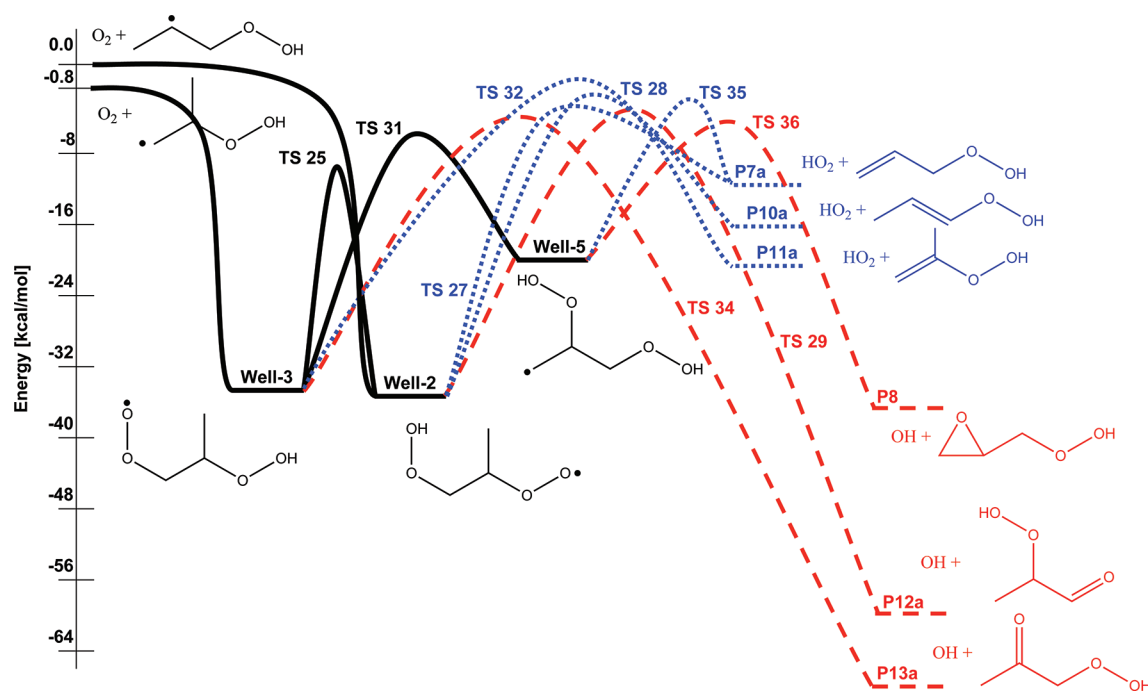


Figure 5. $\text{O}_2 + 3\text{-hydroperoxyl-2-propyl}$ (QOOH-2) and $\text{O}_2 + 2\text{-hydroperoxyl-1-propyl}$ (QOOH-3) potential energy surface. The solid black lines represent the entrance and isomerization channels; the dashed red lines represent the $\text{OH} + \text{keto-hydroperoxide}$ product channels; the dotted blue lines represent the $\text{HO}_2 + \text{alkenyl hydroperoxides}$ product channels.

this with two sets of calculations as follows: In the first set, $\text{RO}_2\text{-1}$ and QOOH-1 were treated as distinct species. In the second set, we consider one fewer chemical species in relating the phenomenological rate coefficients to the eigenvalues and eigenvectors of the full master equation. This corresponds to merging the two species $\text{RO}_2\text{-1}$ and QOOH-1 into the ROO' species. In this set of calculations, the rate coefficient for the $\text{O}_2 + n\text{-propyl} \rightarrow \text{RO}_2\text{-1}$ is assumed to be equal to the rate coefficient for $\text{O}_2 + n\text{-propyl} \rightarrow \text{ROO}'$ times $1/(K+1)$, where K is the $\text{RO}_2\text{-1} \leftrightarrow \text{QOOH-1}$ equilibrium constant, with $K < 1$. Similarly, the rate coefficient for the $\text{O}_2 + n\text{-propyl} \rightarrow \text{QOOH-1}$ is equal to the rate coefficient for the $\text{O}_2 + n\text{-propyl} \rightarrow \text{ROO}'$ times $K/(K+1)$.

For each pressure, the temperature at which the eigenvalues λ_4 merged into the continuum was determined, T_λ . For temperatures greater than T_λ , all rate constants starting from $\text{RO}_2\text{-1}$ were computed as the appropriate rate constant starting from ROO' , scaled by $1/(K+1)$. Similarly, all the rate constants starting from QOOH-1 were computed as the rate constants starting from ROO' , scaled by $K/(K+1)$. For isomerization from $\text{RO}_2\text{-1}$ to QOOH-1, this approach obviously would not work. Instead, to capture the underlying physical chemistry while still maintaining $\text{RO}_2\text{-1}$ and QOOH-1 as distinct species, this isomerization rate constant was replaced for $T > T_\lambda$ with a value faster than the collision rate (e.g., 10^{10} s^{-1}). This approach uses the correct rate constant for isomerization at $T < T_\lambda$, and it forces these two species to equilibrate faster than the time scale of the reaction for $T > T_\lambda$. Care must be taken not to make this equilibration rate constant too fast, because any rate constant much beyond the collision limit could exacerbate the numerical stiffness of the resulting system of ordinary differential equations.

The upturn around 950 K in the rate coefficient for $\text{O}_2 + n\text{-propyl} \rightarrow \text{QOOH-1}$ in Figure 8 arises from our need to introduce an approximate scheme for defining the rate constant for temperatures beyond which it exists and from numerical

ambiguities at temperatures near the crossing temperature. This upturn is more pronounced at lower pressures and is less pronounced at higher pressures. It is difficult to predict exactly when the transition from one method to the other should occur. In all likelihood, the transition becomes significant once the ratio of the largest chemically significant eigenvalue to the first continuum eigenvalue, λ_5/λ_4 , falls below a certain value, e.g., $\lambda_5/\lambda_4 < 2$, which occurs around 800 K at 1 atm. Under this assumption, the effective rate coefficient will undergo a smooth transition from one method to the other. Nonetheless, it is encouraging that these two approaches are in quantitative agreement at the temperature at which λ_4 crosses into the continuum.

The rate coefficients for the decomposition of $\text{RO}_2\text{-1}$, QOOH-1, and QOOH-2 are provided in the Supporting Information. Starting from $\text{RO}_2\text{-1}$, the dominant reaction above 450 K is dissociation back to $\text{O}_2 + n\text{-propyl}$. The rate coefficient for isomerization to QOOH-1 is smaller but of a similar order of magnitude. The rate constants for decomposition to $\text{HO}_2 + \text{propene}$ and $\text{OH} + \text{propylene oxide}$ are 2 and 4 orders of magnitude smaller, respectively, than for dissociation back to $\text{O}_2 + n\text{-propyl}$.

Starting from QOOH-1, the dominant reaction is isomerization back to $\text{RO}_2\text{-1}$, followed by decomposition to $\text{O}_2 + n\text{-propyl}$. As with $\text{RO}_2\text{-1}$, the rate coefficients for decomposition to $\text{HO}_2 + \text{propene}$ and $\text{OH} + \text{propylene oxide}$ are several orders of magnitude smaller. Because the rate constant for isomerization between $\text{RO}_2\text{-1}$ and QOOH-1 is large, and because the rate constants for decomposition to $\text{HO}_2 + \text{propene}$ and $\text{OH} + \text{propylene oxide}$ are comparatively much smaller, $\text{RO}_2\text{-1}$ and QOOH-1 rapidly equilibrate with $\text{O}_2 + n\text{-propyl}$. This rapid equilibration combined with the absence of any fast decomposition reactions is what allows the QOOH-1 concentration to build up enough for $\text{O}_2 + \text{QOOH-1}$ to become significant.

Table 7. Species for 3-Hydroperoxyl-2-propyl (QOOH-2) + O₂ and 2-Hydroperoxyl-1-propyl (QOOH-3) + O₂ Potential Energy Surface^b

#	Species Name	Structure	Relative energy ^a	T1 diagnostic	#	Species Name	Structure	Relative energy ^a	T1 diagnostic
QOOH-2	3-hydroperoxyl-2-propyl + O ₂		0.0	0.013, 0.007	P10b	propen-1-oxy + OH + HO ₂		0.4	0.020, 0.006, 0.037
QOOH-3	2-hydroperoxyl-1-propyl + O ₂		-0.8	0.013, 0.007	P11a	2-propene-hydroperoxide + HO ₂		-20.7	0.013, 0.037
Well-2	1-methyl-2-hydroperoxy-ethylperoxy		-34.7	0.026	P11b	propen-2-oxy + OH + HO ₂		-1.1	0.020, 0.006, 0.037
Well-3	2-hydroperoxy-n-propylperoxy		-34.4	0.026	P12a	1-formyl-ethyl-hydroperoxide + OH		-60.7	0.014, 0.006
Well-5	2,3-dihydroperoxy-n-propyl		-19.9	0.014	P12b	1-formyl-ethoxy + OH + OH		-16.4	0.032, 0.006
P7a	allylhydroperoxide + HO ₂		-13.3	0.012, 0.037	P13a	acetyl-methyl-hydroperoxide + OH		-65.4	0.014, 0.006
P7b	allyloxy + OH + HO ₂		29.9	0.020, 0.006, 0.037	P13b	acetyl-methoxy + OH + OH		-20.4	0.034, 0.006
P8a	oxiranyl-methyl-hydroperoxide + OH		-36.5	0.013, 0.006	P14	OH + CH ₂ O + vinyl-hydroperoxide ^b		-32.7	0.006, 0.016, 0.014
P8b	Oxiranyl-methoxy + OH + OH		8.4	0.018, 0.006	P15	OH + oxetanyl-3-hydroperoxide ^b		-35.6	0.006, 0.012
P10a	1-propene-hydroperoxide + HO ₂		-16.3	0.013, 0.037					

^aAll energies are 0 K E₀, relative to O₂ + QOOH-2, in kcal/mol. ^bProducts P14 and P15 are not included in the RRKM/ME calculations.

The reactions starting from QOOH-2 are quite different. Unlike RO₂-1 and QOOH-1, the barriers for decomposition to HO₂ + propene and OH + propylene oxide, TS8 and TS9, respectively, are lower in energy than the barrier for isomerization back to RO₂-1, TS3. Consequently, the largest rate constant is decomposition to OH + propylene oxide, with decomposition to HO₂ + propene an order of magnitude smaller. Isomerization to RO₂-1 is the next largest rate constant, and it is roughly 4 orders of magnitude smaller. Even though little QOOH-2 is formed, either directly from O₂ + *n*-propyl or via isomerization from RO₂-1 or QOOH-1, what little is formed quickly decays to OH + propylene oxide. In this sense, the QOOH-2 channel acts as a delay in the conversion of O₂ + *n*-propyl to OH + propylene oxide.

3.3.2. O₂ + Isopropyl. The results of the master equation calculations for O₂ + isopropyl are summarized in Figure 9. In contrast to O₂ + *n*-propyl, the O₂ + isopropyl reaction yields comparatively little QOOH-3, which is consistent with the prediction made in section 3.1.1, because the barrier for isomerization is above the reactants in energy. Virtually all of the initial adduct either is stabilized into RO₂-2 or decomposes to HO₂ + propene. Due to the high barrier for isomerization, neither QOOH-3 nor OH + propylene oxide is formed at an appreciable rate, which is consistent with similar results for O₂ + ethyl.

3.3.3. HO₂ + Propene. In the RRKM/ME calculations, the bimolecular product channels are treated as irreversible sinks; consequently, rate constants for the conversion of one product channel into another must be computed separately. As seen from Figures 2 and 3, it is possible for HO₂ + propene to skip QOOH-2 and QOOH-3 and go directly to OH + propylene oxide. HO₂ + propene is the dominant bimolecular product channel in O₂ + propyl chemistry, and the concentration of these two species is relatively high in C3 flames. The reaction HO₂ + propene → OH + propylene oxide can accelerate ignition phenomena, because it converts relatively unreactive HO₂ radicals to more reactive OH radicals. For both QOOH-2 and QOOH-3, the barrier to dissociation to OH + propylene oxide is lower in energy than the barrier to return to HO₂ + propene. Under combustion-relevant conditions, the majority of HO₂ + propene that combines to form a unimolecular intermediate goes directly to OH + propylene oxide. However, the rate coefficient for this chemically activated product channel is still smaller than the rate coefficient for H-abstraction: HO₂ + propene → H₂O₂ + allyl.

As part of their broader work on propene oxidation chemistry, Walker and co-workers provided experimental rate coefficients for this reaction.⁴⁷ In those experiments, tetramethylbutane thermally decomposed to two *tert*-butyl radicals

in the presence of oxygen and propene in 60 Torr of N₂. Product yields were measured by gas chromatography. The *tert*-butyl radicals were assumed to react with the oxygen to form HO₂ + isobutene. The rate constant for HO₂ + propene → OH + propylene oxide was obtained indirectly by fitting a larger reaction mechanism to the product yields. The computed rate coefficients for this reaction are shown in Figure 10. As can be seen from the plot, the agreement between the present work and the experimental rate constants is excellent. The computed rate coefficients are within a factor of 2, which is well within the stated experimental error.

Table 8. Transition States for 3-Hydroperoxyl-2-propyl (QOOH-2) + O₂ and 2-Hydroperoxyl-1-propyl (QOOH-3) + O₂ Potential Energy Surface^a

no.	reactions	relative energy ^a	T1 diagnostic
TS 23	QOOH-2 + O ₂ ↔ Well-2	barrierless	
TS 24	QOOH-3 + O ₂ ↔ Well-3	barrierless	
TS 25	Well-2 ↔ Well-3	−10.5	0.050
TS 26	Well-2 ↔ Well-5 ^b	1.5	0.025
TS 27	Well-2 ↔ P7a	−2.9	0.031
TS 28	Well-2 ↔ P10a	−2.6	0.031
TS 29	Well-2 ↔ P12a	−4.0	0.022
TS 30	Well-2 ↔ P13a ^b	6.1	0.018
TS 31	Well-3 ↔ Well-5	−7.1	0.024
TS 32	Well-3 ↔ P11a	−0.6	0.031
TS 33	Well-3 ↔ P12a ^b	9.2	0.019
TS 34	Well-3 ↔ P13a	−5.7	0.024
TS 35	Well-5 ↔ P7a	−1.5	0.020
TS 36	Well-5 ↔ P8a	−5.2	0.021
TS 37	Well-5 ↔ P14 ^b	7.1	0.026
TS 38	Well-5 ↔ P15 ^b	2.7	0.020

^aAll energies are 0 K *E*₀, relative to O₂ + QOOH-2, in kcal/mol.

^bTransition states are not included in the RRKM/ME calculations: TS 26, TS 30, TS 33, TS 37, and TS 38.

3.3.4. O₂ + QOOH-1. The RRKM/ME results for O₂ + QOOH-1 are shown in Figure 11. Analysis of the eigenpairs in preliminary calculations showed that the eigenvalues for the decomposition of Well-4 merge into the continuum around 700 K, creating some difficulties for its inclusion in the overall kinetic scheme. However, these calculations also showed that the rate of formation of Well-4 was negligible. Therefore, for simplicity and improved numerical accuracy, Well-4 was treated as a product in the RRKM/ME calculations at all temperatures. To maintain HO₂ + allyl hydroperoxide and OH + oxiranylmethyl hydroperoxide as available chemically activated product channels, the high-pressure limit rate constants for the thermal decomposition of Well-4 to HO₂ + allyl hydroperoxide and to OH + oxiranylmethyl hydroperoxide, *k*₂₁ and *k*₂₂, respectively, were computed. The pressure-dependent rate coefficient for O₂ + QOOH-1 → OH + oxiranylmethyl hydroperoxide was estimated as the computed pressure-dependent rate coefficient for O₂ + QOOH-1 → Well-4, scaled by *k*₂₂/(*k*₂₁ + *k*₂₂). Similarly, the computed pressure-dependent rate coefficient for O₂ + QOOH-1 → Well-4, scaled by *k*₂₁/(*k*₂₁ + *k*₂₂) was added to the computed pressure-dependent rate coefficient for O₂ + QOOH-1 → HO₂ + allyl hydroperoxide to account for the additional flux through Well-4.

Because the RRKM/ME code treats bimolecular product channels as irreversible sinks, it does not matter whether the product channel is represented as OH + 2-formylethyl hydroperoxide or OH + OH + 2-formylethoxy. However, it does matter which channel is used for the asymmetric tunneling correction. We have chosen OH + 2-formylethyl hydroperoxide, which is what is shown in Figure 11.

As expected, the dominant product at these pressures is Well-1, followed by OH + 2-formylethyl hydroperoxide. At 400 K at 1 atm, the rate coefficient for concerted HO₂ elimination is 2 orders of magnitude lower; above 1000 K at 1 atm, however, the HO₂ channel becomes the dominant bimolecular channel, consistent with the entropic considerations described in section 3.1.3. This switching temperature increases with pressure.

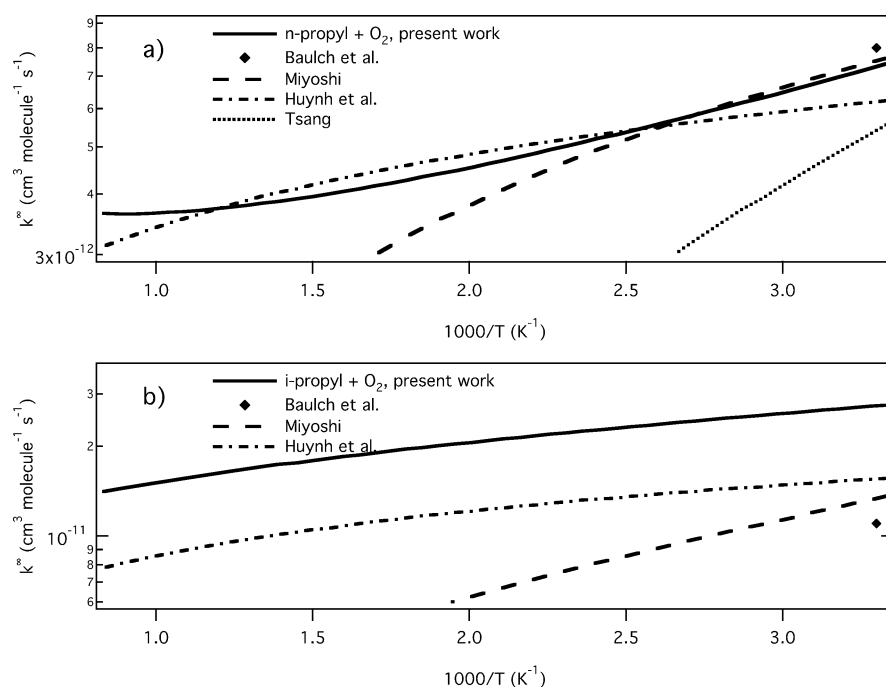


Figure 6. High-pressure limit rate constants for O₂ + C₃H₇. (a) O₂ + *n*-C₃H₇ rate coefficients. (b) O₂ + *i*-C₃H₇ rate coefficients.

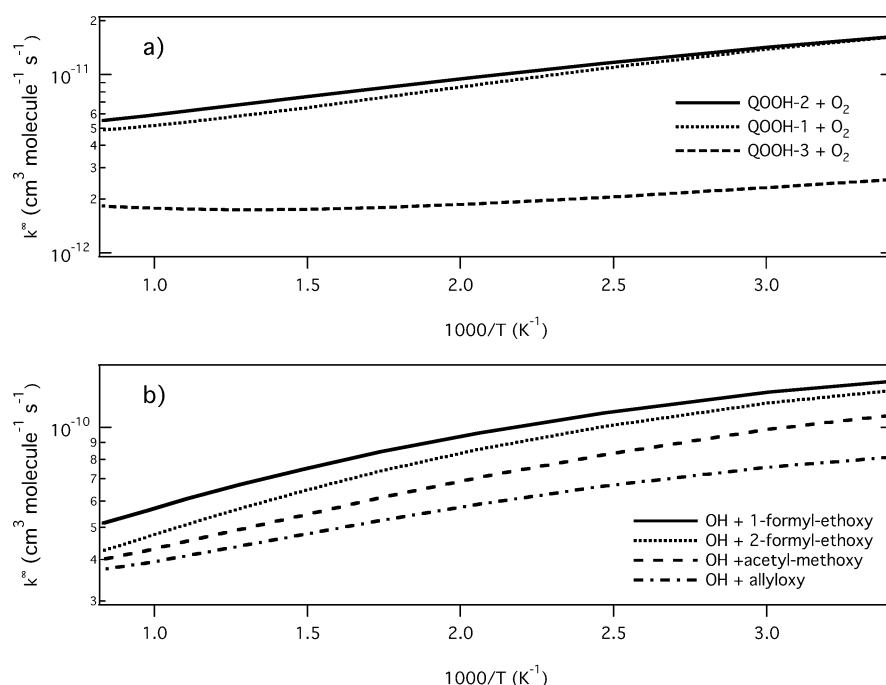


Figure 7. High-pressure limit rate constants. (a) $\text{O}_2 + \text{C}_3\text{H}_7\text{O}_2$ rate coefficients. (b) $\text{OH} + \text{C}_3\text{H}_6\text{O}_2$ and $\text{OH} + \text{C}_3\text{H}_6\text{O}_3$ rate coefficients. The rate coefficient for $\text{OH} + \text{allyloxy}$ ⁴⁴ is also used for $\text{OH} + \text{propen-1-oxy}$ and $\text{OH} + \text{propen-2-oxy}$; the rate coefficient for $\text{OH} + \text{acetylmethoxy}$ is also used for $\text{OH} + \text{oxiranylmethoxy}$.

Starting from Well-1, the dominant rate constant at low temperatures is decomposition to $\text{OH} + 2\text{-formylethyl hydroperoxide}$. At 1 atm, the decomposition back to $\text{O}_2 + \text{QOOH-1}$ becomes the dominant rate constant above 650 K. This switching temperature is a weak function of pressure: at 0.01 atm, the switching temperature is ~ 700 K, and at 100 atm it is ~ 600 K. The $\text{OH} + 2\text{-formylethyl hydroperoxide}$ channel is still within an order of magnitude of $\text{O}_2 + \text{QOOH-1}$ at higher temperatures. The rate constant for $\text{HO}_2 + \text{allyl hydroperoxide}$ is roughly 2 orders of magnitude smaller than the largest rate constant.

3.3.5. $\text{O}_2 + \text{QOOH-2}$ and $\text{O}_2 + \text{QOOH-3}$. The results for $\text{O}_2 + \text{QOOH-2}$ are shown in Figure 12. As discussed in section 3.1.4, none of the decomposition channels available to Well-2 and Well-3 feature a six-membered ring transition state. Owing to the absence of any low-lying product channels, a significantly greater percentage of the initial $\text{C}_3\text{H}_7\text{O}_4^\ddagger$ adduct is stabilized into the initial well. For $\text{O}_2 + \text{QOOH-2}$, the dominant channel is Well-2. The rate constants for the chain branching channels are several orders of magnitude smaller than that for stabilization into Well-2.

The results for $\text{O}_2 + \text{QOOH-3}$ (not shown) are qualitatively similar. The dominant product channel is Well-3, with the rate constants for the formation of Well-2 and Well-5 roughly 2 and 4 orders of magnitude smaller, respectively. The fastest bimolecular product channel is $\text{OH} + \text{OH} + \text{acetylmethoxy}$, which is 2 orders of magnitude smaller than formation of Well-3. The other OH and HO_2 channels are several orders of magnitude smaller.

Starting with Well-2, the dominant channel is decomposition back to $\text{O}_2 + \text{QOOH-2}$, followed by isomerization to Well-3. Starting with Well-3, the dominant channel is decomposition back to $\text{O}_2 + \text{QOOH-3}$, followed by isomerization to Well-2. Starting with Well-5, the dominant channel is decomposition to $\text{OH} + \text{oxiranylmethyl hydroperoxide}$, followed by Well-3 and $\text{HO}_2 + \text{allyl hydroperoxide}$.

In general, the effect of $\text{O}_2 + \text{QOOH-2}$ and $\text{O}_2 + \text{QOOH-3}$ on chain branching is muted. In essence, $\text{O}_2 + \text{QOOH-2}$, $\text{O}_2 + \text{QOOH-3}$, Well-2, Well-3, and Well-5 will rapidly equilibrate. Once equilibration is established, the bimolecular product channels become more significant.

3.4. Effect of $\text{O}_2 + \text{QOOH}$ on Chain Branching. As outlined in the Introduction, it is an open question as to whether the rate constants for $\text{O}_2 + \text{QOOH}$ are large enough to offset the low concentrations of QOOH. To answer this question and to quantify the temperature and pressure range in which $\text{O}_2 + \text{QOOH}$ could have a positive effect on chain branching, a simple kinetic mechanism was developed. This mechanism consists of 24 reversible reactions for $\text{C}_3\text{H}_7\text{O}_2$ chemistry and 54 reversible reactions for the $\text{C}_3\text{H}_7\text{O}_4$ chemistry. The individual reactions are summarized in Tables 10–18; the rate coefficients and thermochemistry parameters are provided in the Supporting Information.

This mechanism is not intended to form a complete mechanism for propyl oxidation. Indeed, neither initiation reactions nor secondary reactions between products are included. The purpose of this simplified mechanism is solely to determine the conditions under which the second O_2 addition may contribute to chain branching. The inclusion of secondary chemistry, with a particular emphasis on $\text{O}_2 + \text{QOOH}$ versus $\text{RO}_2 + \text{RH}$ as a source of chain branching, will be discussed in detail in a separate paper.⁶

A constant-temperature, constant-pressure batch reactor was used to model the system. The initial mole fractions were $y_{n\text{-propyl}} = 10^{-15}$ and $y_{\text{O}_2} = 10^{-1}$, with the remaining bulk He. This ultralow radical concentration was chosen so that the difference between constant temperature and pressure simulations and constant volume and internal energy simulations would be negligible. Additionally, radical–radical interactions can be safely neglected at these concentrations, which becomes important once secondary chemistry is included.⁶ The simulations were

Table 9. Computed High-Pressure Limit Rate Coefficients^a

reaction	A	n	E _a	k(750 K)
TS1: R1 + O ₂ → RO ₂ -1	2.1 × 10 ⁻¹²	0.5	-560	3.8 × 10 ⁻¹²
	3.4 × 10 ⁻¹²	-0.5	0.0 ^b	3.9 × 10 ⁻¹²
	1.5 × 10 ⁻¹²	-1.6	100 ^c	2.1 × 10 ⁻¹²
TS2: RO ₂ -1 → QOOH-1	2.0 × 10 ¹⁰	2.8	9950	1.6 × 10 ⁴
	9.3 × 10 ¹⁰	0.0	11580 ^b	1.8 × 10 ⁴
	3.1 × 10 ¹¹	0.0	10570 ^c	6.2 × 10 ⁴
	7.5 × 10 ¹⁰	1.6	11560 ^d	3.6 × 10 ⁴
	8.9 × 10 ¹⁰	2.4	10580 ^e	3.3 × 10 ⁴
	1.7 × 10 ¹¹	1.3	10930 ^f	5.5 × 10 ⁴
TS3: RO ₂ -1 → QOOH-2	8.0 × 10 ⁹	5.3	11790	2.6 × 10 ²
	3.8 × 10 ¹¹	0.0	15410 ^b	4.5 × 10 ²
	1.0 × 10 ¹²	1.1	15160 ^c	1.8 × 10 ³
	4.0 × 10 ¹¹	0.0	15130 ^d	4.9 × 10 ²
	6.5 × 10 ¹⁰	2.9	13530 ^e	4.1 × 10 ²
	7.9 × 10 ¹¹	1.5	14650 ^f	1.7 × 10 ³
TS10: R2 + O ₂ → RO ₂ -2	1.4 × 10 ⁻¹¹	-0.3	-100	1.7 × 10 ⁻¹¹
	8.6 × 10 ⁻¹²	-0.5	0.0 ^c	9.9 × 10 ⁻¹²
	2.1 × 10 ⁻¹²	-0.8	-270 ^a	3.7 × 10 ⁻¹²
TS11: RO ₂ -2 → QOOH-3	1.6 × 10 ¹⁰	5.2	12930	1.1 × 10 ²
	3.6 × 10 ¹¹	0.0	17370 ^b	3.1 × 10 ¹
	9.7 × 10 ¹¹	1.1	16870 ^c	1.2 × 10 ²
	1.5 × 10 ¹²	0.0	16720 ^g	3.2 × 10 ²
TS16: O ₂ + QOOH-1 → Well-1	3.1 × 10 ⁻¹²	0.1	-540	6.2 × 10 ⁻¹²
TS23: O ₂ + QOOH-2 → Well-2	4.2 × 10 ⁻¹²	-0.1	-350	6.9 × 10 ⁻¹²
TS24: O ₂ + QOOH-3 → Well-3	1.2 × 10 ⁻¹²	0.5	-420	1.8 × 10 ⁻¹²
TS38: P7b → P7a	3.3 × 10 ⁻¹¹	-0.2	-210 ^h	4.6 × 10 ⁻¹¹
TS39: P8a → P8b	3.4 × 10 ⁻¹¹	-0.2	-270	5.2 × 10 ⁻¹¹
TS39: P9b → P9a	4.3 × 10 ⁻¹¹	-0.5	-140	6.0 × 10 ⁻¹¹
TS41: P10b → P10a	3.3 × 10 ⁻¹¹	-0.2	-210 ^h	4.6 × 10 ⁻¹¹
TS42: P11b → P11a	3.3 × 10 ⁻¹¹	-0.2	-210 ^h	4.6 × 10 ⁻¹¹
TS43: P12b → P12a	5.3 × 10 ⁻¹¹	-0.5	-100	7.0 × 10 ⁻¹¹
TS38: P13b → P13a	3.4 × 10 ⁻¹¹	-0.2	-270	5.2 × 10 ⁻¹¹

^aThe rate coefficients are of the form $k(T) = A(T/1000)^n \exp[-E_a/T]$, with A in cm³ molecule⁻¹ s⁻¹ for bimolecular reactions, and s⁻¹ for unimolecular reactions, and E_a in Kelvin. The superscript indicates rate coefficients reproduced from literature values: ^bHuynh,¹⁷ ^cMiyoshi,²⁰ ^dSharma,²⁴ ^eZhang,²² ^fVillano,²³ ^gGoldsmith,⁴⁶ ^hThe high-pressure limit for TS35 is estimated by analogy from TS32.⁴⁶

performed at pressures of 0.1, 1, and 10 atm, and temperatures between 400 and 1200 K, using Chemkin 4.1.⁴⁸ The simulations were integrated until a final time of 1000 s. Experimentally, most of the OH is consumed before 10 ms, so OH yields beyond this value would be of little physical relevance.⁴

One important aspect of the C₃H₇O₂ chemistry in Tables 10 and 11 is that these reactions are all chain propagating. Consequently, the total number of radicals would remain constant throughout the simulation if only those reactions are included. In contrast, the C₃H₇O₄ chemistry in Tables 12–18 includes several chain branching steps. Therefore, the total number of radicals can increase or decrease, depending upon the kinetics and thermodynamics of these reactions.

To make the comparison across different temperatures and pressures meaningful, it is useful to have a chemically relevant time constant, rather than some arbitrary fixed reference time. The characteristic time constant we have chosen is the time required for P9a, 2-formylethyl hydroperoxide, to reach a maximum. Values for this time constant depend strongly on the

composition, temperature, and pressure; for the initial conditions considered here, typical values are between 0.1 ms and 1 s.

The increase in the total number of radicals is a useful metric for assessing the significance for second O₂ addition in ignition chemistry. This result is quantified in Figure 13, which illustrates how the peak in chain branching changes with temperature at various pressures. The “percent increase in the total number of radicals” is determined by summing over the mole fraction of all the radical species and then normalizing this value by the initial mole fraction of *n*-propyl. The percent increase is then this sum minus unity, multiplied by 100. In the absence of chain branching, this value would be zero. Any value greater than zero is a measure of the chain branching that arises from inclusion of the QOOH + O₂ chemistry. The percent increase in the total number of radicals increases with pressure, from 2% at 0.1 atm to 9% at 10 atm. The temperature at which the maximum occurs also increases, from 640 K at 0.1 atm to 740 K at 10 atm. The corresponding time constants for P9a to reach a maximum are 100, 10, and 1 ms at 0.1, 1.0, and 10.0 atm, respectively.

It is important to stress that the percent increase in radical concentration should not be confused with a corresponding percent decrease in the ignition delay. Low-temperature oxidation is a complex process involving numerous feedback loops, even under low-radical concentrations. Although the increase in the number of radicals illustrated in Figure 13 may seem small, these small changes are amplified in ignition delay. For example, at 750 K and 10 atm, the percent increase in radicals is roughly 9%, but when the O₂ + QOOH reactions are coupled with a larger mechanism for low-temperature oxidation chemistry, the ignition delay is decreased by nearly an order of magnitude.⁶

The increase in radicals due to O₂ + QOOH is confined to the temperatures between 600 and 900 K at pressures between 0.1 and 10 atm. The maximum in radical production can be attributed to two opposing trends: the rate constants for thermal decomposition of keto-hydroperoxides favor higher temperatures, whereas the O₂ + R ↔ RO₂ equilibrium constant favors lower temperatures.

At 500 K, QOOH reacts with O₂ to form hydroperoxyalkylperoxy radicals, which in turn dissociate to OH + keto-hydroperoxides, but the rate coefficients for the thermal decomposition of keto-hydroperoxides are too low at this temperature for there be significant chain branching. Increasing the temperature increases the rate of keto-hydroperoxide decomposition, thereby increasing chain branching.

At 1000 K, the O₂ + R ↔ RO₂ equilibrium constant significantly favors the bimolecular reactants. Additionally, the rate coefficients for the thermal dissociation of RO₂ and QOOH are competitive with the rate constants for O₂ addition. The combination of these two effects yields significantly less QOOH available to react with O₂. Lowering the temperature shifts the equilibrium in favor of the RO₂/QOOH admixture, and it decreases the rate of RO₂/QOOH dissociation, which increases the amount of QOOH available to react with O₂, thereby increasing chain branching.

Increasing the pressure has three main effects. First, increasing the pressure at constant mole fraction of O₂ shifts the O₂ + R ↔ RO₂ equilibrium in favor of RO₂. Second, increasing the pressure increases the rate coefficient for the collisional stabilization to the initial adduct. The combination of these two effects significantly increases the concentration of QOOH. Third, increasing the pressure favors bimolecular reactions. As mentioned above, the unimolecular decomposition of RO₂ and

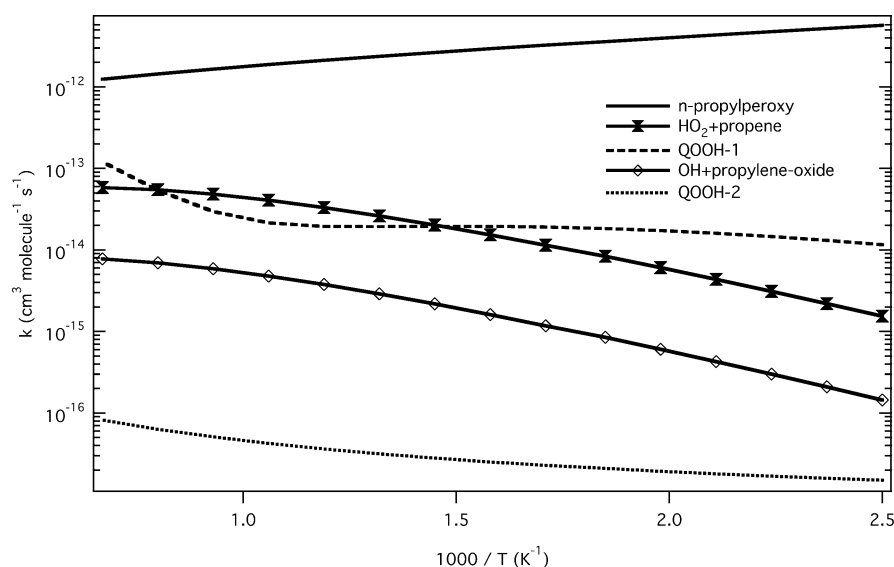


Figure 8. RRKM/ME results for $\text{O}_2 + n\text{-propyl}$ in 1 atm He. The top line is the rate constant for collisional stabilization of $n\text{-propylperoxy}$. The dashed and dotted lines correspond to chemically activated formation of QOOH, and the symbols correspond to chemically activated bimolecular product channels.

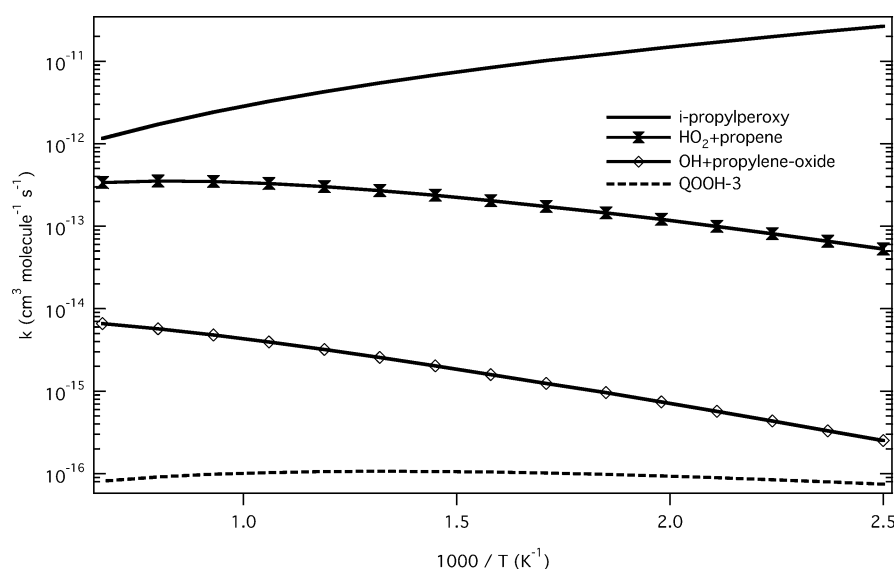


Figure 9. RRKM/ME results for $\text{O}_2 + \text{isopropyl}$ in 1 atm He. The top line is the rate constant for collisional stabilization of isopropylperoxy. The lines with symbols are chemically activated bimolecular product channels. The dashed line is QOOH-3.

QOOH becomes competitive with (and ultimately faster than) bimolecular O_2 addition at higher temperatures. Increasing the pressure will offset this competition at a given temperature, because the net rate of $\text{O}_2 + \text{QOOH}$ is proportional to pressure whereas the decomposition channels are not.

Changing the pressure also has a fourth, more subtle effect. Increasing the pressure increases the rate coefficient for collisional stabilization of hydroperoxyalkylperoxy radicals at the expense of the formally direct chain-branching reaction. The hydroperoxyalkylperoxy radicals will decompose to OH + keto-hydroperoxides, and (provided there is sufficient thermal energy) the keto-hydroperoxides will decompose to OH + oxy-radicals. Thus, the pressure dependence of the $\text{O}_2 + \text{QOOH}$ rate coefficients has little impact on the total amount of chain branching, because all of the products ultimately decompose, but it has a significant impact on when the chain branching occurs. Chain branching due to the formally direct reactions,

$\text{O}_2 + \text{QOOH-1} \rightarrow \text{OH} + \text{OH} + \text{oxy-radical}$, is significant on the nanosecond-to-microsecond time scale, whereas chain branching due to the sequential reactions, $\text{O}_2 + \text{QOOH-1} \rightarrow \text{OOQOOH} \rightarrow \text{keto-hydroperoxide} + \text{OH} \rightarrow \text{keto-oxy radical} + \text{OH} + \text{OH}$, is significant on the millisecond-to-second time scale.

Figure 14a shows the equilibrium constants between $\text{R} + \text{O}_2$, RO_2 , and QOOH for the $n\text{-propyl}$ system. Figure 14b shows the forward rate constants for the formation of keto-hydroperoxide (solid line) at 1 atm and alkyl hydroperoxide (dotted line). For the temperature range of interest (e.g., 600–900 K), the equilibrium constant for isomerization from RO_2 to QOOH-1 (the solid line in Figure 14a) is between 10^{-5} and 10^{-3} . The activation energies for $\text{RO}_2 + \text{RH} \rightarrow \text{ROOH} + \text{R}$ are typically between 17 and 20 kcal/mol,⁴⁹ whereas the activation energies for $\text{O}_2 + \text{QOOH} \rightarrow \text{products}$ are typically between 7 and 9 kcal/mol. Therefore, the rate constant for $\text{O}_2 + \text{QOOH-1} \rightarrow \text{Well-1}$ is between 10^4 and 10^6 times larger than

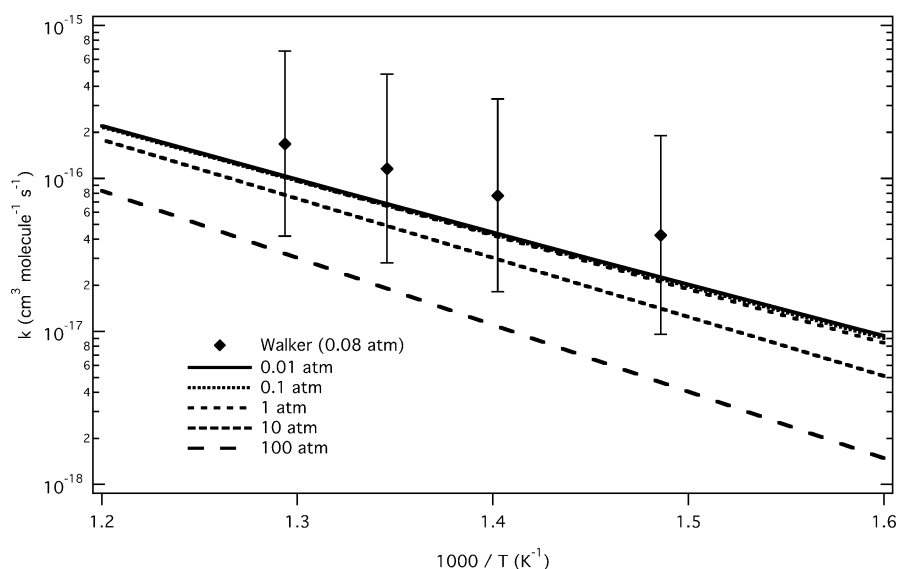


Figure 10. RRKM/ME results for $\text{HO}_2 + \text{propene} \rightarrow \text{OH} + \text{propylene oxide}$.

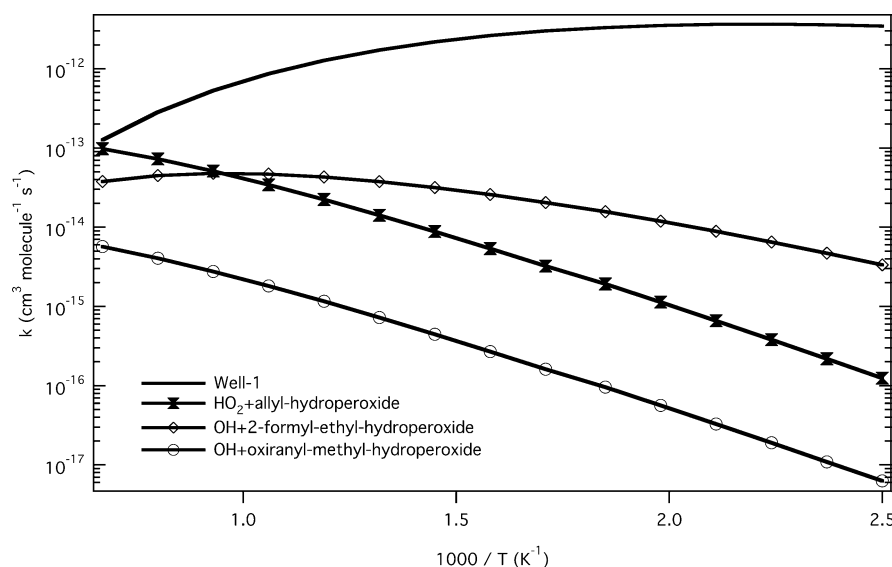


Figure 11. RRKM/ME results for $\text{O}_2 + \text{QOOH-1}$ in 1 atm He. The top line is the rate constant for collisional stabilization of Well-1. The lines with symbols are chemically activated bimolecular product channels.

the rate constants for $\text{C}_3\text{H}_7\text{O}_2 + \text{C}_3\text{H}_8 \rightarrow \text{C}_3\text{H}_7\text{OOH} + \text{C}_3\text{H}_7$ (i.e., the solid line versus the dotted line in Figure 14b) over the same temperature range. Thus, if we assume that $\text{RO}_2\text{-1}$ and QOOH-1 are equilibrated, then in a stoichiometric propane/air mixture between 600 and 900 K the net rate of $\text{O}_2 + \text{QOOH} \rightarrow \text{products}$ will be more than an order of magnitude faster than the net rate of $\text{RO}_2 + \text{RH} \rightarrow \text{ROOH} + \text{R}$. Consequently, the $\text{O}_2 + \text{QOOH}$ reactions are expected to have a significant impact on ignition delays at low temperatures. A comparison of the role of $\text{O}_2 + \text{QOOH}$ versus $\text{RO}_2 + \text{RH}$ in low-temperature ignition is addressed in detail in the companion paper.⁶

3.5. Uncertainty Due to Hindered-Rotor Model. As detailed in section 3.3, the 1D hindered-rotor model used in this paper is a poor description of the actual conformational space. To minimize the error associated with this model, some of the barriers were chosen from the quasi-cyclic lowest-energy structure, and the remaining barriers were taken from the straight-chain conformer. To test the significance of this crude

approximation on the phenomenological rate coefficients, sample calculations were performed for $\text{O}_2 + \text{QOOH-1}$ at 1 and 10 atm. In one set of calculations, all the barriers were taken from the quasi-cyclic structure; in the other set of calculations, all the barriers were taken from the straight-chain conformer. A plot of these calculations is available in the Supporting Information.

At 400 K, the rate constants for the bimolecular channels that were calculated with the high rotational barriers are almost a factor of 2 larger than the rate constants calculated with the low rotational barriers; the rate constants for collisional stabilization were unaffected. At 1200 K, in contrast, the situation is reversed. The difference in the rate constants for the bimolecular channels is negligible, whereas the unimolecular stabilization rate constants with the high rotational barriers are almost a factor of 2 smaller than the corresponding low rotational barrier rate constants. Because the rotational barriers used in the present work represent an average of the two extremes, we can

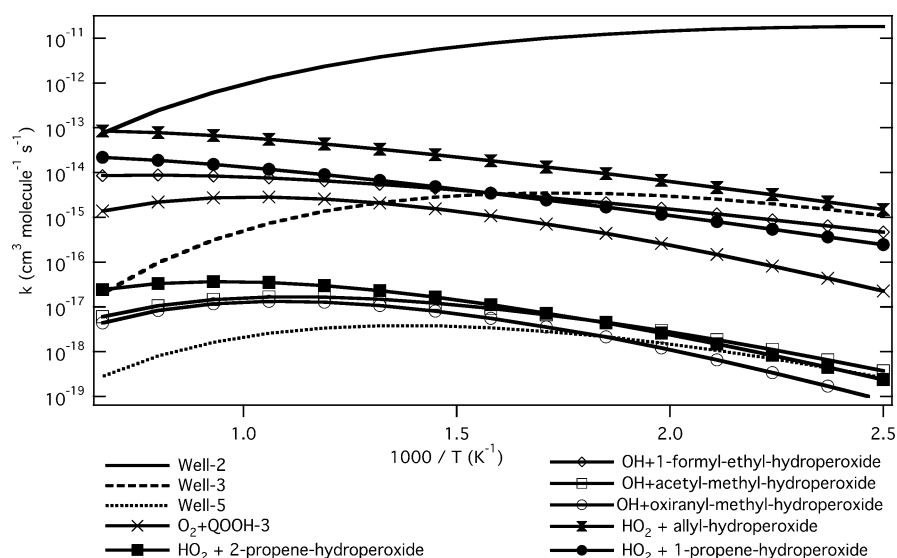


Figure 12. RRKM/ME results for $\text{O}_2 + \text{QOOH-2}$ in 1 atm He. The top line is the rate constant for collisional stabilization of Well-2. The lines with symbols are chemically activated bimolecular product channels.

Table 10. $\text{C}_3\text{H}_7\text{O}_2$ Mechanism: $\text{O}_2 + n\text{-Propyl}$

Reaction	#
$\text{O}_2 + \text{CH}_3\text{CH}_2\text{CH}_2\cdot \rightleftharpoons \text{CH}_3\text{CH}_2\text{CH}_2\text{OO}\cdot$	[R1]
$\text{CH}_3\text{CH}_2\text{CH}_2\text{OO}\cdot \rightleftharpoons \text{CH}_3\text{CH}_2\text{CH}_2\text{OOH}$	[R2]
$\text{CH}_3\text{CH}_2\text{CH}_2\text{OOH} \rightleftharpoons \text{CH}_3\text{CH}_2\text{CH}_2\text{OO}\cdot$	[R3]
$\text{CH}_3\text{CH}_2\text{CH}_2\text{OOH} \rightleftharpoons \text{HO}_2 + \text{CH}_2=\text{CHCH}_3$	[R4]
$\text{CH}_3\text{CH}_2\text{CH}_2\text{OOH} \rightleftharpoons \text{OH} + \text{CH}_3\text{CH}_2\text{CH}_2\text{O}$	[R5]
$\text{CH}_3\text{CH}_2\text{CH}_2\text{OO}\cdot \rightleftharpoons \text{CH}_3\text{CH}_2\text{CH}_2\text{OOH}$	[R6]
$\text{CH}_3\text{CH}_2\text{CH}_2\text{OOH} \rightleftharpoons \text{CH}_3\text{CH}_2\text{CH}_2\text{OO}\cdot$	[R7]
$\text{CH}_3\text{CH}_2\text{CH}_2\text{OOH} \rightleftharpoons \text{HO}_2 + \text{CH}_2=\text{CHCH}_3$	[R8]
$\text{CH}_3\text{CH}_2\text{CH}_2\text{OOH} \rightleftharpoons \text{OH} + \text{CH}_3\text{CH}_2\text{CH}_2\text{O}$	[R9]
$\text{CH}_3\text{CH}_2\text{CH}_2\text{OOH} \rightleftharpoons \text{CH}_3\text{CH}_2\text{CH}_2\text{OO}\cdot$	[R10]
$\text{CH}_3\text{CH}_2\text{CH}_2\text{OOH} \rightleftharpoons \text{HO}_2 + \text{CH}_2=\text{CHCH}_3$	[R11]
$\text{CH}_3\text{CH}_2\text{CH}_2\text{OOH} \rightleftharpoons \text{OH} + \text{CH}_3\text{CH}_2\text{CH}_2\text{O}$	[R12]
$\text{CH}_3\text{CH}_2\text{CH}_2\text{OOH} \rightleftharpoons \text{HO}_2 + \text{CH}_2=\text{CHCH}_3$	[R13]
$\text{CH}_3\text{CH}_2\text{CH}_2\text{OOH} \rightleftharpoons \text{OH} + \text{CH}_3\text{CH}_2\text{CH}_2\text{O}$	[R14]
$\text{HO}_2 + \text{CH}_2=\text{CHCH}_3 \rightleftharpoons \text{OH} + \text{CH}_3\text{CH}_2\text{CH}_2\text{O}$	[R15]

conclude that the uncertainty in the phenomenological rate coefficients due to the hindered rotor approximation is less than a factor of 2, and the intermediate barrier rate constants are probably within 50% of the correct ones.

Based upon these sample calculations, the uncertainty in the partition functions is roughly equivalent to the uncertainty in other factors such as the electronic structure calculations of the energies, the normal-mode frequencies, the treatment of energy transfer, and the neglect of other anharmonicities.

Table 11. $\text{C}_3\text{H}_7\text{O}_2$ Mechanism: $\text{O}_2 + \text{Isopropyl}$

Reaction	#
$\text{O}_2 + \text{CH}_3\text{CH}(\text{CH}_3)\cdot \rightleftharpoons \text{CH}_3\text{CH}(\text{CH}_3)\text{OO}\cdot$	[R16]
$\text{CH}_3\text{CH}(\text{CH}_3)\text{OO}\cdot \rightleftharpoons \text{CH}_3\text{CH}(\text{CH}_3)\text{OOH}$	[R17]
$\text{CH}_3\text{CH}(\text{CH}_3)\text{OOH} \rightleftharpoons \text{CH}_3\text{CH}(\text{CH}_3)\text{OO}\cdot$	[R18]
$\text{CH}_3\text{CH}(\text{CH}_3)\text{OOH} \rightleftharpoons \text{HO}_2 + \text{CH}_2=\text{CHCH}_3$	[R19]
$\text{CH}_3\text{CH}(\text{CH}_3)\text{OOH} \rightleftharpoons \text{OH} + \text{CH}_3\text{CH}(\text{CH}_3)\text{O}$	[R20]
$\text{CH}_3\text{CH}(\text{CH}_3)\text{OO}\cdot \rightleftharpoons \text{CH}_3\text{CH}(\text{CH}_3)\text{OOH}$	[R21]
$\text{CH}_3\text{CH}(\text{CH}_3)\text{OOH} \rightleftharpoons \text{CH}_3\text{CH}(\text{CH}_3)\text{OO}\cdot$	[R22]
$\text{CH}_3\text{CH}(\text{CH}_3)\text{OOH} \rightleftharpoons \text{HO}_2 + \text{CH}_2=\text{CHCH}_3$	[R23]
$\text{CH}_3\text{CH}(\text{CH}_3)\text{OOH} \rightleftharpoons \text{OH} + \text{CH}_3\text{CH}(\text{CH}_3)\text{O}$	[R24]

Table 12. $\text{C}_3\text{H}_7\text{O}_4$ Mechanism: $\text{O}_2 + \text{QOOH-1}$ and Well-1 Decomposition

Reactions	#
$\text{O}_2 + \text{CH}_3\text{CH}_2\text{CH}_2\text{OO}\cdot \rightleftharpoons \text{CH}_3\text{CH}_2\text{CH}_2\text{OOO}\cdot$	[R25]
$\text{CH}_3\text{CH}_2\text{CH}_2\text{OOO}\cdot \rightleftharpoons \text{OH} + \text{CH}_3\text{CH}_2\text{CH}_2\text{OO}\cdot$	[R26]
$\text{CH}_3\text{CH}_2\text{CH}_2\text{OOO}\cdot \rightleftharpoons \text{HO}_2 + \text{CH}_3\text{CH}_2\text{CH}_2\text{OO}\cdot$	[R27]
$\text{CH}_3\text{CH}_2\text{CH}_2\text{OOO}\cdot \rightleftharpoons \text{OH} + \text{CH}_3\text{CH}_2\text{CH}_2\text{OO}\cdot$	[R28]
$\text{CH}_3\text{CH}_2\text{CH}_2\text{OOO}\cdot \rightleftharpoons \text{OH} + \text{CH}_3\text{CH}_2\text{CH}_2\text{OO}\cdot$	[R29]
$\text{CH}_3\text{CH}_2\text{CH}_2\text{OOO}\cdot \rightleftharpoons \text{HO}_2 + \text{CH}_3\text{CH}_2\text{CH}_2\text{OO}\cdot$	[R30]
$\text{CH}_3\text{CH}_2\text{CH}_2\text{OOO}\cdot \rightleftharpoons \text{OH} + \text{CH}_3\text{CH}_2\text{CH}_2\text{OO}\cdot$	[R31]

Table 13. $C_3H_7O_4$ Mechanism: $O_2 + QOOH-2$

Reactions	#
$O_2 + \text{isopropyl-QOOH-2} \rightleftharpoons \text{isopropyl-QOOH-2-O}_2$	[R32]
$\text{isopropyl-QOOH-2-O}_2 \rightleftharpoons \text{isopropyl-QOOH-2-O}_2^*$	[R33]
$\text{isopropyl-QOOH-2-O}_2^* \rightleftharpoons \text{isopropyl-QOOH-2-O}_2^{\ddagger}$	[R34]
$\text{isopropyl-QOOH-2-O}_2^{\ddagger} \rightleftharpoons \text{isopropyl-QOOH-2-O}_2^*$	[R35]
$\text{isopropyl-QOOH-2-O}_2^* \rightleftharpoons \text{isopropyl-QOOH-2-O}_2^{\ddagger}$	[R36]
$\text{isopropyl-QOOH-2-O}_2^{\ddagger} \rightleftharpoons \text{isopropyl-QOOH-2-O}_2^*$	[R37]
$\text{isopropyl-QOOH-2-O}_2^* \rightleftharpoons \text{isopropyl-QOOH-2-O}_2^{\ddagger}$	[R38]
$\text{isopropyl-QOOH-2-O}_2^{\ddagger} \rightleftharpoons \text{isopropyl-QOOH-2-O}_2^*$	[R39]
$\text{isopropyl-QOOH-2-O}_2^* \rightleftharpoons \text{isopropyl-QOOH-2-O}_2^{\ddagger}$	[R40]
$\text{isopropyl-QOOH-2-O}_2^{\ddagger} \rightleftharpoons \text{isopropyl-QOOH-2-O}_2^*$	[R41]

Table 14. $C_3H_7O_4$ Mechanism: $O_2 + QOOH-3$

Reactions	#
$O_2 + \text{isopropyl-QOOH-3} \rightleftharpoons \text{isopropyl-QOOH-3-O}_2$	[R42]
$\text{isopropyl-QOOH-3-O}_2 \rightleftharpoons \text{isopropyl-QOOH-3-O}_2^*$	[R43]
$\text{isopropyl-QOOH-3-O}_2^* \rightleftharpoons \text{isopropyl-QOOH-3-O}_2^{\ddagger}$	[R44]
$\text{isopropyl-QOOH-3-O}_2^{\ddagger} \rightleftharpoons \text{isopropyl-QOOH-3-O}_2^*$	[R45]
$\text{isopropyl-QOOH-3-O}_2^* \rightleftharpoons \text{isopropyl-QOOH-3-O}_2^{\ddagger}$	[R46]
$\text{isopropyl-QOOH-3-O}_2^{\ddagger} \rightleftharpoons \text{isopropyl-QOOH-3-O}_2^*$	[R47]
$\text{isopropyl-QOOH-3-O}_2^* \rightleftharpoons \text{isopropyl-QOOH-3-O}_2^{\ddagger}$	[R48]
$\text{isopropyl-QOOH-3-O}_2^{\ddagger} \rightleftharpoons \text{isopropyl-QOOH-3-O}_2^*$	[R49]
$\text{isopropyl-QOOH-3-O}_2^* \rightleftharpoons \text{isopropyl-QOOH-3-O}_2^{\ddagger}$	[R50]

Consequently, improving the electronic energies has reached a point of diminishing return for this system; commensurate to the effort required, further adjustments to the potential energy surface may not necessarily improve the overall accuracy. To decrease the global uncertainty in the phenomenological rate coefficients, more sophisticated treatments are required for many additional factors such as the hindered-rotor partition functions.

Table 15. $C_3H_7O_4$ Mechanism: Well-2 Decomposition

Reactions	#
$\text{isopropyl-QOOH-2} \rightleftharpoons \text{isopropyl-QOOH-2}^*$	[R51]
$\text{isopropyl-QOOH-2}^* \rightleftharpoons \text{isopropyl-QOOH-2}^{\ddagger}$	[R52]
$\text{isopropyl-QOOH-2}^{\ddagger} \rightleftharpoons \text{isopropyl-QOOH-2}^*$	[R53]
$\text{isopropyl-QOOH-2}^* \rightleftharpoons \text{isopropyl-QOOH-2}^{\ddagger}$	[R54]
$\text{isopropyl-QOOH-2}^{\ddagger} \rightleftharpoons \text{isopropyl-QOOH-2}^*$	[R55]
$\text{isopropyl-QOOH-2}^* \rightleftharpoons \text{isopropyl-QOOH-2}^{\ddagger}$	[R56]
$\text{isopropyl-QOOH-2}^{\ddagger} \rightleftharpoons \text{isopropyl-QOOH-2}^*$	[R57]
$\text{isopropyl-QOOH-2}^* \rightleftharpoons \text{isopropyl-QOOH-2}^{\ddagger}$	[R58]

Table 16. $C_3H_7O_4$ Mechanism: Well-3 Decomposition

Reactions	#
$\text{isopropyl-QOOH-3} \rightleftharpoons \text{isopropyl-QOOH-3}^*$	[R59]
$\text{isopropyl-QOOH-3}^* \rightleftharpoons \text{isopropyl-QOOH-3}^{\ddagger}$	[R60]
$\text{isopropyl-QOOH-3}^{\ddagger} \rightleftharpoons \text{isopropyl-QOOH-3}^*$	[R61]
$\text{isopropyl-QOOH-3}^* \rightleftharpoons \text{isopropyl-QOOH-3}^{\ddagger}$	[R62]
$\text{isopropyl-QOOH-3}^{\ddagger} \rightleftharpoons \text{isopropyl-QOOH-3}^*$	[R63]
$\text{isopropyl-QOOH-3}^* \rightleftharpoons \text{isopropyl-QOOH-3}^{\ddagger}$	[R64]
$\text{isopropyl-QOOH-3}^{\ddagger} \rightleftharpoons \text{isopropyl-QOOH-3}^*$	[R65]

Table 17. $C_3H_7O_4$ Mechanism: Well-5 Decomposition

Reactions	#
$\text{isopropyl-QOOH-5} \rightleftharpoons \text{isopropyl-QOOH-5}^*$	[R66]
$\text{isopropyl-QOOH-5}^* \rightleftharpoons \text{isopropyl-QOOH-5}^{\ddagger}$	[R67]
$\text{isopropyl-QOOH-5}^{\ddagger} \rightleftharpoons \text{isopropyl-QOOH-5}^*$	[R68]
$\text{isopropyl-QOOH-5}^* \rightleftharpoons \text{isopropyl-QOOH-5}^{\ddagger}$	[R69]
$\text{isopropyl-QOOH-5}^{\ddagger} \rightleftharpoons \text{isopropyl-QOOH-5}^*$	[R70]
$\text{isopropyl-QOOH-5}^* \rightleftharpoons \text{isopropyl-QOOH-5}^{\ddagger}$	[R71]

4. PROPYL RADICAL AS COMBUSTION ARCHETYPE

The results in section 3.4 clearly highlight the significance of six-membered ring transition states for intramolecular H-abstraction in low-temperature chain branching. The low-lying

transition states that lead to the formation of QOOH-1 and the decomposition of Well-1 are responsible for the growth in radical species exhibited in Figure 13. The same calculations performed in Figure 13 were repeated for O_2 + isopropyl. The higher barrier for the 1,4s H-transfer reaction that leads to QOOH-3, and the lack of any low-lying decomposition pathways for Well-2 and Well-3 resulted in negligible chain

Table 18. $C_3H_6O_3$ and $C_3H_6O_2$ Decomposition

	[R72]
	[R73]
	[R74]
	[R75]
	[R76]
	[R77]
	[R78]

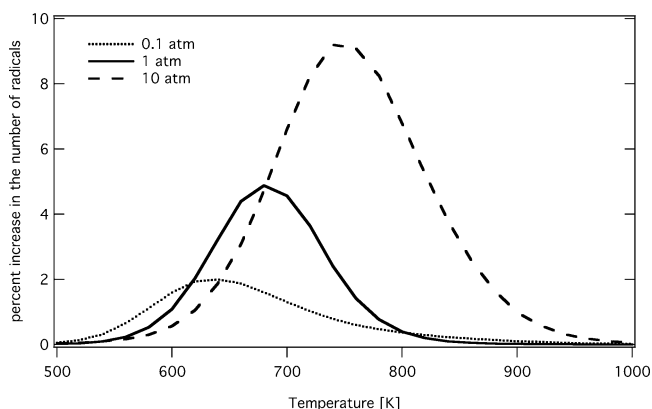


Figure 13. Increase in the number of radicals as a function of temperature and pressure.

branching, with the percent increase in the total number of radicals being less than 0.01%. The difference in performance between *n*-propyl and isopropyl can be linked entirely to the six-membered ring transition states.

The chain-branching results obtained for O_2 + *n*-propyl should be even more pronounced for larger alkyl radicals.²³ Consider *n*-butyl as the next example. The 1,5s H-transfer reaction from *n*-butylperoxy to form 4-hydroperoxy-2-butyl should have a lower barrier than the 1,5p H-transfer from RO_2 -1 to QOOH-1, because the *n*-butyl QOOH isomer is a secondary radical. As such, it will be more stable relative to *n*-butylperoxy than QOOH-1 is to RO_2 -1. Based upon the results in Figure 6 and 9a, the rate constant for oxygen addition to secondary radicals is generally larger than addition to primary radicals (this trend is in contrast to results for alkyl + alkyl reactions, in which steric hindrance in the secondary radical lowers the rate coefficient by roughly a factor of 2;⁷ the reverse in this trend for O_2 + alkyl radicals is probably due to hydrogen bonding in the transition-state region). Therefore, simply because this QOOH is a secondary radical, more of it will be formed, more of it will be available after equilibration with RO_2 , and the rate of O_2 + QOOH consumption will increase. The combination of these three effects should yield even higher increases in chain branching. In this regard, even though *n*-propyl is the smallest alkyl radical to exhibit the autoignition characteristics of larger alkyl radicals, *n*-butyl is perhaps more characteristic and hence a better combustion archetype. Furthermore, with *n*-butyl and larger alkyl radicals, 1,6 H-transfer reactions are possible, which should have barriers similar to 1,5 H-transfer reactions.²⁴

5. CONCLUSIONS

A theoretical investigation of the kinetics of the O_2 + QOOH bimolecular reaction and its impact on low-temperature chain branching has been performed over a wide range of temperatures and pressures relevant for combustion modeling. The results indicated that chain branching is significant only when the isomerization from a peroxy radical to a hydroperoxyalkyl radical proceeds via a cyclic transition state with six or more members.

The reaction sequence O_2 + QOOH \rightarrow OOQOOH \rightarrow OH + keto-hydroperoxide \rightarrow OH + OH + oxy-radical and the corresponding formally direct reaction O_2 + QOOH \rightarrow OH + OH + oxy-radical are responsible for growth of the radical pool

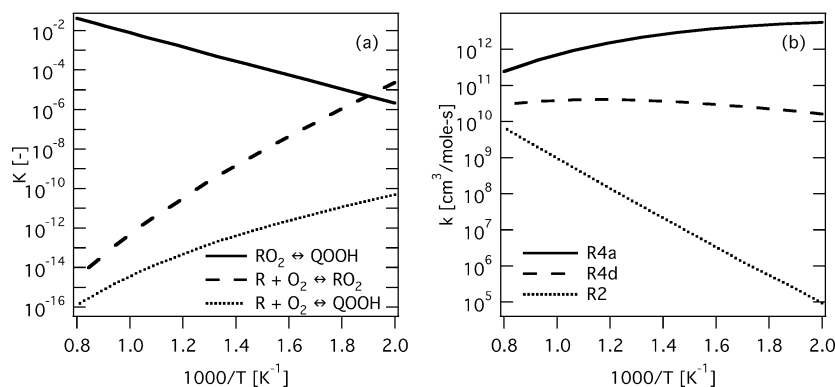


Figure 14. (a) Equilibrium constants for *n*-propyl + O_2 ($R + O_2$), *n*-propylperoxy (RO_2), and 3-hydroperoxypropyl (QOOH). (b) Forward rate coefficients for hydroperoxide formation in the two competing chain-branching sequences: the solid line, [R4a], is for O_2 + QOOH-1 \rightarrow 3-hydroperoxy-*n*-propylperoxy at 1 atm; the dashed line, [R4d], is for O_2 + QOOH-1 \rightarrow OH + OH + 2-formylethoxy at 1 atm; the dotted line, [R2], is the sum of the four rate coefficients for $n/i-C_3H_7O_2 + C_3H_8 \rightarrow n/i-C_3H_7OOH + n/i-C_3H_7$.⁴⁹

in the first few milliseconds after the initial reaction. The contribution of these reactions is maximized in the temperature range 600–900 K.

Below 500 K, virtually all of the excited RO_2^+ adduct is stabilized into *n*-propylperoxy. The small amount of QOOH that is formed reacts with O_2 to form hydroperoxypropylperoxy radicals. These species decompose to OH + keto-hydroperoxides, but the keto-hydroperoxides are stable at this temperature, so this channel does not contribute to chain branching. Above 1000 K, the lack of QOOH is attributed to (i) an $\text{O}_2 + \text{R} \leftrightarrow \text{RO}_2$ equilibrium constant that strongly favors the reactants, and (ii) the rate constants for RO_2 and QOOH thermal dissociation are competitive with O_2 addition.

The uncertainty in the phenomenological rate coefficients due to the 1D hindered-rotor model is about a factor of 1.5. Future efforts to decrease the uncertainty in the model will need to consider many different factors including the treatment of the multidimensional nature of the hindered rotations, their coupling to the vibrations, the energy transfer models, the energies of the barriers, and other components of the vibrational anharmonicity. The results confirm that *n*-propyl is the smallest alkyl radical to exhibit the low-temperature combustion properties of larger alkyl radicals, but *n*-butyl is perhaps a truer combustion archetype.

■ ASSOCIATED CONTENT

■ Supporting Information

A CHEMKIN compatible mechanism for the reactions in Tables 10–18 is available. The geometries of the species and transition states are provided. Also included are plots of the $\text{C}_3\text{H}_6\text{O}_3$ and $\text{C}_3\text{H}_6\text{O}_2$ potential energy surfaces, and a plot of the calculated rate constants for $\text{O}_2 + \text{QOOH-1}$ in the hindered-rotor barrier height uncertainty analysis. This material is available free of charge via the Internet at <http://pubs.acs.org>.

■ AUTHOR INFORMATION

Corresponding Author

*E-mail: sjk@anl.gov.

Notes

The authors declare no competing financial interest.

■ ACKNOWLEDGMENTS

We thank members of the Combustion Research Facility at Sandia National Laboratories—particularly Craig Taatjes and James Miller—and Wes Allen at University of Georgia for useful comments and suggestions during the preparation of this manuscript. This work is supported by Division of Chemical Sciences, Geosciences, and Biosciences, the Office of Basic Energy Science (BES) of the U.S. Department of Energy (DOE), with the portion at MIT through contract DE-FG02-98ER14914 and jointly by the CEFRC through contract DE-SC0001198, and the portion at Argonne through contract DE-AC02-06CH11357 as part of the Argonne-Sandia Consortium on High-Pressure Combustion Chemistry; FWP# 2009 ANL 59044. C.F.G. gratefully acknowledges fellowship support from the National Science Foundation and the Alexander von Humboldt Foundation.

■ REFERENCES

- (1) Zádor, J.; Taatjes, C. A.; Fernandes, R. X. *Prog. Energy Combust. Sci.* **2011**, *37*, 371.
- (2) Westbrook, C. K.; Pitz, W. J. Lawrence Livermore National Laboratory, Combustion Chemistry, 2012.
- (3) Curran, H. J.; Simmie, J. M. National University of Ireland, Galway, Combustion Chemistry Centre, 2012.
- (4) DeSain, J. D.; Klippenstein, S. J.; Miller, J. A.; Taatjes, C. A. *J. Phys. Chem. A* **2003**, *107*, 4415.
- (5) DeSain, J. D.; Clifford, E. P.; Taatjes, C. A. *J. Phys. Chem. A* **2001**, *105*, 3205.
- (6) Goldsmith, C. F.; Klippenstein, S. J.; Green, W. H. Manuscript in preparation, 2011.
- (7) Klippenstein, S. J.; Georgievskii, Y.; Harding, L. B. *Phys. Chem. Chem. Phys.* **2006**, *8*, 1133.
- (8) Harding, L. B.; Klippenstein, S. J.; Jasper, A. W. *Phys. Chem. Chem. Phys.* **2007**, *9*, 4055.
- (9) DeSain, J. D.; Taatjes, C. A.; Miller, J. A.; Klippenstein, S. J.; Hahn, D. K. *Faraday Discuss.* **2001**, *119*, 101.
- (10) Estupiñán, E. G.; Klippenstein, S. J.; Taatjes, C. A. *J. Phys. Chem. B* **2005**, *109*, 8374.
- (11) Estupiñán, E. G.; Smith, J. D.; Tezaki, A.; Klippenstein, S. J.; Taatjes, C. A. *J. Phys. Chem. A* **2007**, *111*, 4015.
- (12) Huang, H.; Merthe, D. J.; Zádor, J.; Jusinski, L. E.; Taatjes, C. A. *Proc. Combust. Inst.* **2011**, *33*, 293.
- (13) Fernandes, R. X.; Zador, J.; Jusinski, L. E.; Miller, J. A.; Taatjes, C. A. *Phys. Chem. Chem. Phys.* **2009**, *11*, 1320.
- (14) Wijaya, C. D.; Sumathi, R.; Green, W. H. Jr. *J. Phys. Chem. A* **2003**, *107*, 4908.
- (15) Green, W. H.; Wijaya, C. D.; Yelvington, P. E.; Sumathi, R. *Mol. Phys.* **2004**, *102*, 371.
- (16) Merle, J. K.; Hayes, C. J.; Zalyubovsky, S. J.; Glover, B. G.; Miller, T. A.; Hadad, C. M. *J. Phys. Chem. A* **2005**, *109*, 3637.
- (17) Huynh, L. K.; Carstensen, H. H.; Dean, A. M. *J. Phys. Chem. A* **2010**, *114*, 6594.
- (18) Bozzelli, J. W.; Chen, C.-C. *Personal communication*, 2008.
- (19) Zhang, F.; Dibble, T. S. *J. Phys. Chem. A* **2011**, *115*, 655.
- (20) Miyoshi, A. *J. Phys. Chem. A* **2011**, *115*, 3301.
- (21) Montgomery, J. A.; Frisch, M. J.; Ochterski, J. W.; Petersson, G. A. *J. Chem. Phys.* **1999**, *110*, 2822.
- (22) Zhang, F.; Dibble, T. S. *Phys. Chem. Chem. Phys.* **2011**, *13*, 17969.
- (23) Villano, S. M.; Huynh, L. K.; Carstensen, H. H.; Dean, A. M. *J. Phys. Chem. A* **2011**, *115*, 13425.
- (24) Sharma, S.; Raman, S.; Green, W. H. *J. Phys. Chem. A* **2010**, *114*, 5689.
- (25) Martin, J. M. L. *Chem. Phys. Lett.* **1996**, *259*, 669.
- (26) Feller, D.; Dixon, D. A. *J. Chem. Phys.* **2001**, *115*, 3484.
- (27) Miller, J. A.; Klippenstein, S. J. *J. Phys. Chem. A* **2003**, *107*, 7783.
- (28) Lee, T. J.; Rendell, A. P.; Taylor, P. R. *International Conf in Honor of Professor John A Pople: Forty Years of Quantum Chemistry* **1989**, *94*, 5463.
- (29) Klippenstein, S. J.; Harding, L. B. *Proc. Comb. Inst.* **2009**, *32*, 149.
- (30) Andersson, K.; Malmqvist, P. A.; Roos, B. O. *J. Chem. Phys.* **1992**, *96*, 1218.
- (31) Frisch, M. J.; Trucks, G. W.; Schlegel, H. B.; Scuseria, G. E.; Robb, M. A.; Cheeseman, J. R.; Montgomery, J. A., Jr.; Vreven, T.; Kudin, K. N.; Burant, J. C.; Millam, J. M.; Iyengar, S. S.; Tomasi, J.; Barone, V.; Mennucci, B.; Cossi, M. S. G.; Rega, N.; Petersson, G. A.; Nakatsuji, H.; Hada, M.; Ehara, M.; Toyota, K.; Fukuda, R.; Hasegawa, J.; Ishida, M.; Nakajima, T.; Honda, Y.; Kitao, O.; Nakai, H.; Klene, M.; Li, X.; Knox, J. E.; Hratchian, H. P.; Cross, J. B.; Bakken, V.; Adamo, C.; Jaramillo, J.; Gomperts, R.; Stratmann, R. E.; Yazyev, O.; Austin, A. J.; Cammi, R.; Pomelli, C.; Ochterski, J. W.; Ayala, P. Y.; Morokuma, K.; Voth, G. A.; Salvador, P.; Dannenberg, J. J.; Zakrzewski, V. G.; Dapprich, S.; Daniels, A. D.; Strain, M. C.; Farkas, O.; Malick, D. K.; Rabuck, A. D.; Raghavachari, K.; Foresman, J. B.; Ortiz, J. V.; Cui, Q.; Baboul, A. G.; Clifford, S.; Cioslowski, J.; Stefanov, B. B.; Liu, G.; Liashenko, A.; Piskorz, P.; Komaromi, I.; Martin, R. L.; Fox, D. J.; Keith, T.; Al-Laham, M. A.; Peng, C. Y.; Nanayakkara, A.; Challacombe, M.; Gill, P. M. W.; Johnson, B.; Chen,

W.; Wong, M. W.; Gonzalez, C.; Pople, J. A. *Gaussian 03*; Gaussian, Inc.: Wallingford, CT, 2004.

(32) Werner, H.-J.; Knowles, P. J.; Lindh, R.; Manby, F. R.; Schuetz, M.; et al. *MOLPRO*, version 2006.1, a package of ab initio programs, <http://www.molpro.net>, 2006.

(33) Georgievskii, Y.; Klippenstein, S. J. *J. Phys. Chem. A* **2003**, *107*, 9776.

(34) Klippenstein, S. J. *J. Chem. Phys.* **1992**, *96*, 367.

(35) Georgievskii, Y.; Klippenstein, S. J.; Harding, L. B. *VarReCoF*; Sandia National Laboratories and Argonne National Laboratories, 2006.

(36) Jasper, A. W.; Klippenstein, S. J.; Harding, L. B. *Proc. Combust. Inst.* **2009**, *32*, 279.

(37) Klippenstein, S. J.; Wagner, A. F.; Dunbar, R. C.; Wardlaw, D. M.; Robertson, S. H.; Miller, J. A. *VariFlex*; Sandia National Laboratories and Argonne National Laboratories, 2002.

(38) Joback, K. G. Massachusetts Institute of Technology, 1984.

(39) Barker, J. R.; Ortiz, N. F.; Preses, J. M.; Lohr, L. L.; Maranzana, A.; Stimac, P. J. *MultiWell-2.08 Software*; University of Michigan: Ann Arbor, MI, 2007.

(40) Pitzer, K. S.; Gwinn, W. D. *J. Chem. Phys.* **1942**, *10*, 428.

(41) Johnston, H. S.; Heicklen, J. *J. Phys. Chem.* **1962**, *66*, 532.

(42) Liang, T.; Allen, W. *PROPYL + O₂: Definitive Theory on a Prototype of Hydrocarbon Oxidation*. 7th International Conference on Chemical Kinetics Cambridge, MA, 2011; Paper #266.

(43) Bozzelli, J. W.; Sheng, C. *J. Phys. Chem. A* **2002**, *106*, 1113.

(44) Goldsmith, C. F.; Klippenstein, S. J.; Green, W. H. *Proc. Combust. Inst.* **2011**, *33*, 273.

(45) Baulch, D. L.; Bowman, C. T.; Cobos, C. J.; Cox, R. A.; Just, T.; Kerr, J. A.; Pilling, M. J.; Stocker, D.; Troe, J.; Tsang, W.; Walker, R. W.; Warnatz, J. *J. Phys. Chem. Ref. Data* **2005**, *34*, 757.

(46) Goldsmith, C. F.; Ismail, H.; Abel, P. R.; Green, W. H. *Proc. Combust. Inst.* **2009**, *32*, 139.

(47) Baldwin, R. R.; Hisham, M. W. M.; Walker, R. W. *Proc. Combust. Inst.* **1984**, *26*, 743.

(48) Kee, R. J.; Rupley, F. M.; Miller, J. A.; et al. *CHEMKIN 4.1*; Reaction Design: San Diego, 2007.

(49) Dooley, S.; Burke, M. P.; Chaos, M.; Stein, Y.; Dryer, F. L.; Zhukov, V. P.; Finch, O.; Simmie, J. M.; Curran, H. J. *Int. J. Chem. Kinet.* **2010**, *42*, 527.